Glycoconj J (2011) 28:67–87
DOI 10.1007/s10719-011-9325-6

Systematic analyses of free ceramide species and ceramide species comprising neutral glycosphingolipids by MALDI-TOF MS with high-energy CID

Kouji Tanaka · Masaki Yamada · Keiko Tamiya-Koizumi · Reiji Kannagi · Toshifumi Aoyama · Atsushi Hara · Mamoru Kyogashima

Received: 1 September 2010 / Revised: 11 January 2011 / Accepted: 1 February 2011 / Published online: 12 March 2011

Abstract Free ceramides and glycosphingolipids (GSLs) are important components of the membrane microdomain and play significant roles in cell survival. Recent studies have revealed that both fatty acids and long-chain bases (LCBs) are more diverse than expected, in terms of i) alkyl chain length, ii) hydroxylation and iii) the presence or absence of double bonds. Electrospray ionization mass spectrometry and matrix-assisted laser desorption ionization time-of-flight mass spectrometry (MALDI-TOF MS) have been well utilized to characterize sphingolipids with high throughput, but reports to date have not fully characterized various types of ceramide species such as hydroxyl fatty acids and/or trihydroxy-LCBs of both free ceramides and the constituent ceramides in neutral GSLs. We performed a systematic analysis of both ceramide species, including LCBs with nona-octadeca lengths using MALDI-TOF MS with high-energy collision-induced dissociation (CID) at 20 keV. Using both protonated and sodiated ions, this technique enabled us to propose general rules to discriminate between isomeric and isobaric ceramide species, unrelated to the presence or absence of sugar chains. In addition, this high-energy CID generated ^{3,5}A ions, indicating Hex1-4Hex linkage in the sugar chains. Using this method, we demonstrated distinct differences among ceramide species, including free ceramides, sphingomyelins, and neutral GSLs of glucosylceramides, galactosylceramides, lactosylceramides, globotriaosylceramides and Forssman glycolipids in the equine kidneys.

Keywords Ceramides · Hydroxy-ceramides · Nona-octadeca ceramides · Neutral glycosphingolipids · MALDI-TOF MS · High-energy collision-induced dissociation

Electronic supplementary material The online version of this article (doi:10.1007/s10719-011-9325-6) contains supplementary material, which is available to authorized users.

K. Tanaka · K. Tamiya-Koizumi · R. Kannagi · M. Kyogashima (✉)
Division of Molecular Pathology,
Aichi Cancer Center Research Institute,
Nagoya, Aichi 464-8681, Japan
e-mail: mkyogashi@aichi-cc.jp

K. Tanaka · M. Kyogashima
Department of Oncology, Graduate School of Pharmaceutical Science, Nagoya City University,
Nagoya, Aichi 467-8603, Japan

M. Yamada
Shimadzu Corporation,
Kyoto 604-8511, Japan

T. Aoyama · A. Hara
Department of Metabolic Regulation, Institute on Aging and Adaptation, Shinshu University Graduate School of Medicine,
Matsumoto, Nagano 390-8621, Japan

Introduction

Sphingolipids such as free ceramides and glycosphingolipids (GSLs) are important components of the membrane microdomain and play significant roles in cell survival [1]. Namely, free ceramides, sphingomyelins and their metabolites such as sphingosine and sphingosine-1-phosphate are recognized as signaling molecules involved in cell differentiation, proliferation and apoptosis [2]. GSLs, which are also involved in cell signaling processes, mediate cell–cell adhesion and pathogen entry [3, 4]. Recent studies have revealed that both fatty acids (FAs) and long-chain bases (LCBs) of each class of lipids are

more diverse than expected not only in skin [5], but also in other mammalian organs [6], in terms of i) alkyl chain length, ii) hydroxylation and iii) the presence or absence of double bonds. These factors are considered to affect the geometry of sphingolipids in membrane microdomains of cells [7, 8]. More importantly, evidence is rapidly accumulating to suggest that specific molecular species in a single class of certain lipid exhibit particular functions. For example, the sulfatide possessing C16:0, but not C24:0, was reported to inhibit insulin secretion in rat beta-cells [9], and the lactosylceramide (LacCer) possessing C24:0 and C24:1 were shown to mediate superoxide generation and migration in neutrophils [10]. Interestingly, using the model membranes, Mahfound *et al*. reported that verotoxin-1 binds the lipid vesicles in which globotriaosylceramides (Galα4LacCer, Gb3Cer) with C24:1 was included, although the toxin did not bind the vesicles in which Gb3Cer with C18:0 or C20:0 was included [11].

Liquid chromatography–electrospray ionization mass spectrometry (LC/ESI-MS) and matrix-assisted laser desorption ionization time-of-flight mass spectrometry (MALDI-TOF MS) have been well utilized to characterize sphingolipids with high throughput [5, 6, 12–21], but these reports did not fully characterize ceramide species including hydroxyl FAs (HFAs) and/or trihydroxy-LCBs (tLCBs) of both free ceramides and the constituent ceramides in GSLs. Namely, in the analyses of GSLs these investigations focused on sugar sequences by releasing sugars from the lipid portions [22, 23]; therefore, detailed information regarding the constituent ceramide species in GSLs is limited [20]. We recently demonstrated the diversity of free ceramides, including those with non-octadeca LCBs (NOD-LCBs) using ESI-MS in the negative mode [6]. However, for neutral GSLs, positive mode analysis is more sensitive and informative than negative mode analysis. Therefore, a method for the analysis of free ceramide species and constituent ceramide species in neutral GSLs is urgently needed. In this study, we performed systematic analyses of free ceramides and GSLs, including those with HFAs, tLCBs and/or NOD-LCBs as well as non-hydroxy FAs (NFAs) and octadeca-LCBs (OD-LCBs) using MALDI-TOF MS in the positive mode with high-energy collision-induced dissociation (CID) at 20 keV. This method enabled us to obtain detailed information regarding alkyl chain lengths, the positions of double bonds, hydroxylation status of FAs/LCBs and sugar sequences, as well as information about their linkages, using both ordinary protonated and sodiated ions. Furthermore, we demonstrated distinct differences among ceramide species including free ceramides, sphingomyelins, and GSLs of glucosylceramides (GlcCers), galactosylceramides (GalCer), LacCer, Gb3Cer, globotetraosylceramides (GalNAcβ3Gb3Cer, Gb4Cers) and Forssman glycolipids (GalNAcα3Gb4Cer) in the equine kidneys.

Materials and methods

Materials

The standard ceramides d18:1-C16:0 (ceramide composed of (4E)-sphingenine with C16:0), d18:1-C24:0, d18:0-C24:1 (ceramide composed of sphinganine with C24:1), t18:0-C18:0 (ceramide composed of 4D-hydroxysphinganine with C18:0), and *N*-palmitoyl(D31)-(4E)-sphingenine (d18:1-C16:0(D31)) were obtained from Avanti Polar Lipids (Alabaster, AL). Standard d18:1-C18:0h (d18:1 ceramide with hydroxy-C18:0) and porcine erythrocyte-derived Gb3Cer and Gb4Cer were obtained from Matreya (Pleasant Gap, PA). GlcCer, GalCer, α-galactosidase from green coffee beans, sphingomyelinase from *Bacillus cereus*, and all peptides used as external calibrants were obtained from Sigma-Aldrich (St. Louis, MO). β-*N*-acetylhexosaminidase from Jack beans and α-*N*-acetylgalatosaminidase from *Acremonium* sp. were obtained from Seikagaku Biobusiness (Tokyo, Japan). α-cyano-4-hydroxycinnamic acid (CHCA) and 2,5-dihydroxybenzoic acid (DHB) were obtained from Shimadzu GLC (Tokyo, Japan). All organic solvents used in the experiments were of the highest grade commercially available in Japan.

Preparations of ceramides, sphingomyelins and neutral GSLs from equine kidneys

Sphingomyelins and neutral GSLs were purified from equine kidneys as previously described [6, 24]. Briefly, lipids were extracted with a chloroform–methanol mixture. Ceramides and sphingomyelins were obtained after solvent partition and silica gel (Iatrobeads, Mitsubishi Chemical Medience Corp. Tokyo, Japan) column chromatography. Specifically, ceramides were fractionated using a chloroform-acetone gradient [24, 25] and sphingomyelins were fractionated using a chloroform-methanol gradient. The sphingomyelins were further digested with sphingomyelinase as described [26]. Neutral GSLs were obtained by acetylation and deacetylation methods [27] using Florisil (Wako, Osaka, Japan) column chromatography. Each class of neutral GSL was further purified by silica gel chromatography using a chloroform–methanol gradient [28]. GSLs were analyzed by high-performance thin-layer chromatography (HPTLC) with chloroform:methanol:water (65:25:4, by volume). GlcCers and GalCers were purified using borate-impregnated, preparative HPTLC [24] with chloroform:methanol:water:concentrated ammonia (21:7:0.6:0.1). One to two nmol of Gb3Cers was converted to LacCers by digestion with 0.2 units of the α-galactosidase in 20 m*M*

citrate buffer (pH 4.0) containing 0.1% sodium taurocholate at 37°C for 10 h [29]. Forssman glycolipids were converted to Gb3Cers by sequential digestion with 0.1 units of the α-*N*-acetylgalactosaminidase for 10 h [30] and 0.2 units of the β-*N*-acetylhexosaminidase for 10 h in 20 m*M* citrate buffer (pH 4.0) containing 0.1% sodium taurocholate at 37°C [31].

MALDI-TOF MS, MS/MS

Lipids were prepared as 10–350 pmol/μl solutions in chroloform:methanol (2:1, by volume). One microliter each of matrix (10 mg/ml DHB in chloroform:methanol (2:1) with or without 0.5% trifluoroacetic acid (TFA)) and lipid solution were mixed vigorously and 1 μl of the resultant solution was applied onto the surface of a stainless steel MALDI-TOF plate. All mass spectrometric analyses were performed in positive ion mode using an AXIMA-Performance mass spectrometer (Shimadzu/Kratos,UK) equipped with a nitrogen UV laser (337 nm). The instrument was operated at an acceleration voltage of 20 keV and a pulsed extraction function to improve mass resolution was carefully applied to the *m/z* range 800–1600, based on the sizes of the target molecules. The TOF analyzer was calibrated using the following external calibrants: a dimer of CHCA ($[2M + H]^+$; 379.09), human angiotensin II ($[M + H]^+$; 1046.54), and ACTH18–39 ($[M + H]^+$; 2465.20). Helium gas was used for high-energy CID (20 keV) fragmentation for MS/MS analysis. All mass spectrometric data were acquired and analyzed using MALDI-MS software (Shimadzu/Kratos, UK). The compositions of molecular species from each class of lipid were calculated from the peak areas obtained from spectra as previously described [32].

Nomenclature for the fragmentation of ceramides and GSLs

The nomenclature for the fragmentation of ceramides was modified from Matsuda *et al*. [33]. Ceramides with dihydroxy long-chain bases (dLCBs) possessing a trans-double bond, (abbreviated as d1LCB) are illustrated in Fig. 1a. Ceramides with dLCB without the trans-double bond (d0LCB) and ceramides with tLCBs are illustrated in Fig. 1b. The nomenclature for the fragmentation of GSLs, based on Costello *et al*. [34, 35], is illustrated in Fig. 1c.

Results and discussion

Linear mode and MS/MS analyses of various free ceramides

Figure 2a and b show the linear mode mass spectra for isomers ($C_{42}H_{83}NO_3$) of a d1LCB-NFA (d18:1-C24:0) and d0LCB-NFA (dihydroceramide, d18:0-C24:1). While $[M + H - H_2O]^+$ at *m/z* 632.6 represents a major protonated ion from d18:1-C24:0, the $[M + H]^+$ at *m/z* 650.6 represents a major ion from d18:0-C24:1. $[M + Na]^+$ ions at *m/z* 672.6 were also commonly observed. By ESI-MS analysis of ceramides in either positive or negative mode, $[M + H]^+$ ions [13] or $[M - H]^-$ ions [12] were similarly produced from both ceramides. Using MALDI-TOF MS, dehydration occurs in d1LCB-FAs, but was scarcely seen in d0LCB-FAs, enabling easy discrimination of these isomers in a single mass spectrometry experiment. d0LCB-FAs such as d18:0-Cn:0 often occur as a minor component while d1LCB-FAs such as d18:1-Cn:0 often occur as a major component; if both types of ceramide are similarly observed as $[M + H]^+$, small amounts of d0LCB-FAs may be overlooked, because mono-isotopic ions of the d0LCB-FAs are hidden owing to the second isotopic ions of $[M + H]^+$ from d1LCB-FAs. Indeed, a small amount of d18:0-C18:0h co-existing with d18:1-C18:0h was clearly detected at *m/z* 584.6 (Fig. 2c). This presence was difficult to identify from the spectra of sodiated ions, because the ion at *m/z* 606.5 (d18:0-C18:0h) was masked by the second isotopic ion at the same *m/z* 606.5 from d18:1-C18:0h (Fig. 2c). d0LCB-FAs (dihydroceramides), which were previously considered to be bio-inactive lipids, have recently attracted attention because of their ability to induce autophagy in cells [36]. Therefore, high-sensitivity detection of such species is essential. Figure 2d shows linear mass spectra of tLCB-NFA (t18:0-C18:0). Ions at *m/z* 584.6 $[M + H]^+$ and 606.5 $[M + Na]^+$ were observed with very low amounts of dehydrated ions. This result, together with that obtained when using d0LCB-FAs, indicates that a trans-double bond in LCBs gives sensitivity to dehydration upon MALDI.

Figure 2e and f show MS/MS analyses of protonated ions at *m/z* 632.6 (d18:1-C24:0) and 650.6 (d18:0-C24:1), respectively. As well as small ions at *m/z* 368.4 and 366.4 (a2 + 2H) from C24:0 and C24:1, diagnostic ions (hereinafter, diagnostic ions are used to define LCB/ceramide species of the sphingolipids in this paper) for LCB species at *m/z* 264.3 ($b2 - 2H_2O + 2H$) and 284.2 ($b2 - H_2O + 2H$) were observed (see Supplemental Fig. I). By ESI-MS/MS analysis, a major diagnostic ion from d18:0 could be seen at *m/z* 266.6 [13, 16], close to the ion at *m/z* 264.3 derived from d18:1, but using our MS/MS method, these ions are at *m/z* 284.2, enabling us to discriminate these molecules with ease. This is consistent with the fact that protonated ions from d0LCB-FAs observed in linear mode spectra are less dehydrated than d1LCB-FAs in this instrument. Figure 2g shows the product ions of t18:0-C18:0 at *m/z* 584.6. With a small ion at *m/z* 284.3 (a2 + 2H) from C18:0, characteristic, quadruple ions at *m/z* 318.3 (b2 + 2H), 300.3 ($b2 - H_2O + 2H$) (Supplemental Fig. I) 282.3 ($b2 - 2H_2O + 2H$) and 264.3 ($b2 - 3H_2O + 2H$) were

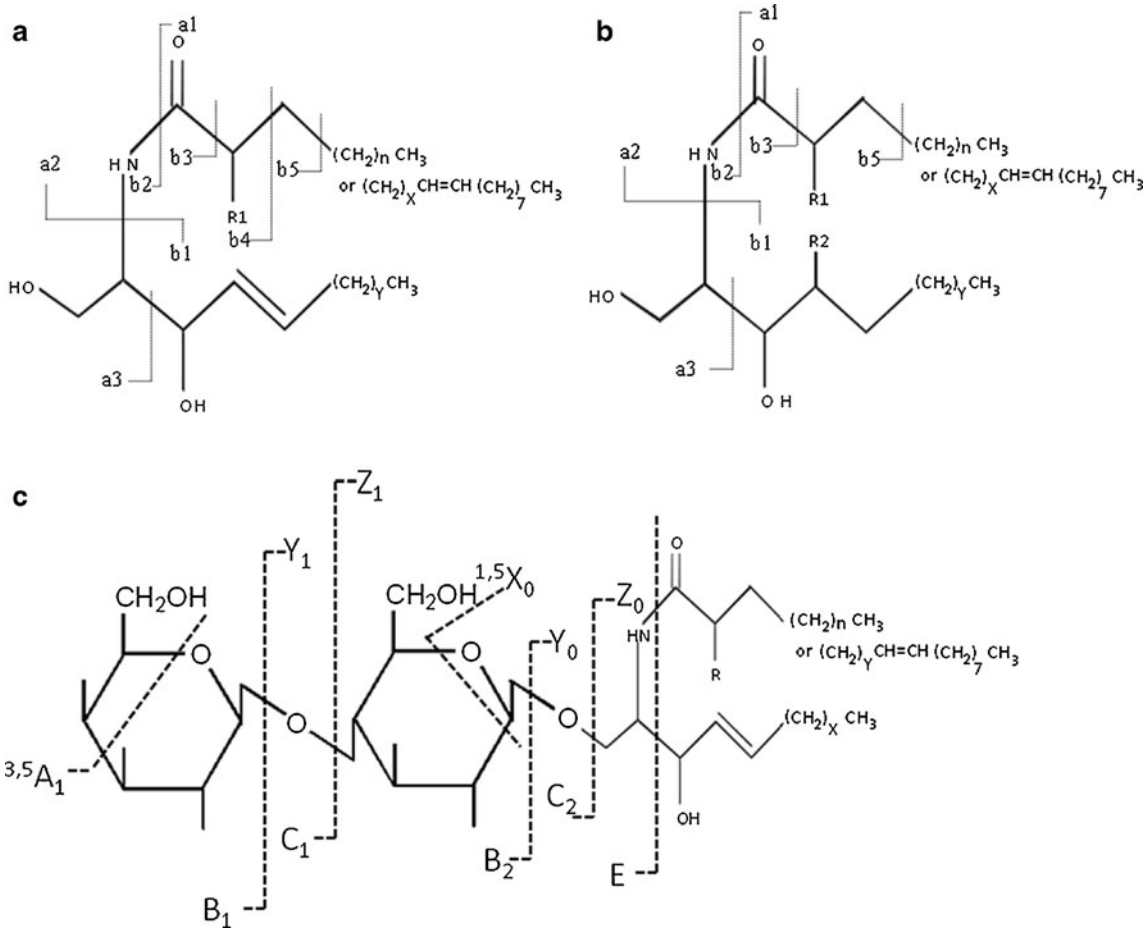

Fig. 1 Fragmentation schemes. **a** and **b** for ion designations of ceramides modified from Matsuda *et al*. 2004 [33]. Species denoted with "a_n" are FA related; species denoted with "b_n" are LCB-related ions. n=13–23, X=9 or 10, Y=10–14, in this experiment. **a** Ceramides possessing d1LCB. R1=H for d1LCB-NFAs and R1=OH for d1LCB-HFAs. **b** Ceramides possessing d0LCB or tLCB. R1=H and R2=H for d0LCB-NFAs, R1=OH and R2=H for d0LCB-HFAs, R1=OH and R2=H for d0LCB-HFAs, R1=H and R2=OH for tLCB-NFAs and R1=OH and R2=OH for tLCB-HFAs. **c** Ion designations of carbohydrates and their linkage portion to ceramides of GSLs, according to Costello *et al*. [34, 35]

generated. We employed the ion at *m/z* 300.3 as a diagnostic ion for t18:0 because it is specific. Compared with the generation efficacies of diagnostic ions at *m/z* 264.3 (d18:1), 284.2 (d18:0) and 300.3 (t18:0), the ion at *m/z* 264.3 was most abundant, and those at *m/z m/z* 284.2 and 303.3 were approximately five-fold less abundant than those at *m/z* 264.3.

Figure 3 shows MS/MS analyses of $[M + Na]^+$ ions from ceramides. A series of ions with a difference of 14 Da (-CH2-) was observed between *m/z* 672.6 and 376.4 (b5 − H + Na), (Fig. 3a) and at *m/z* 672.6 and 378.3 (b5 − H + Na) (Fig. 3b and Supplemental Fig. II); these were generated by charge-remote fragmentation [37, 38]. These types of ions were hardly observed when protonated ions from the ceramides, (especially types of d1LCB-FAs) were chosen as precursor ions. Relatively abundant ions at *m/z* 518.6 and 572.6 among three continuous (-CH2-) less abundant ions (Fig. 3b) corresponded to L and M ions (Supplemental Fig. II), previously reported as lithium adduct ions generated during the analysis of ceramides using fast atom bombardment MS with high-energy CID [39, 40]. These ions indicate the occurrence of a double bond (Δ9) in the nervonic acid (C24:1). Among the series of (-CH_2-) ions, ions at *m/z* 414.4 and 416.4 (a3 − OH + Na) from C24:1 (Fig. 3b) and C24:0 (Fig. 3a) were observed (Supplemental Fig. II). In addition, ions at *m/z* 264.3 were observed among product ions from d18:1-C24:0, which had the same molecular mass as the ions derived from the LCB that was derived from $[M + H - H_2O]^+$ (Fig. 2e and

Fig. 2 Linear mode mass spectra (**a**–**d**) and MS/MS analyses of protonated ions (**e**–**g**) of ceramides. **a** d18:1-C24:0. **b** d18:0-C24:1. **c** d18:1-C18:0h containing a small amount of d18:0-C18:0h. **d** t18:0-C18:0. **e** d18:1-C24:0. **f** d18:0-C24:1. **g** t18:0-C18:0. The protonated ion selected as the precursor was observed at *m/z* 632.6 for (a); 650.6 for (b) and 584.6 for (d)

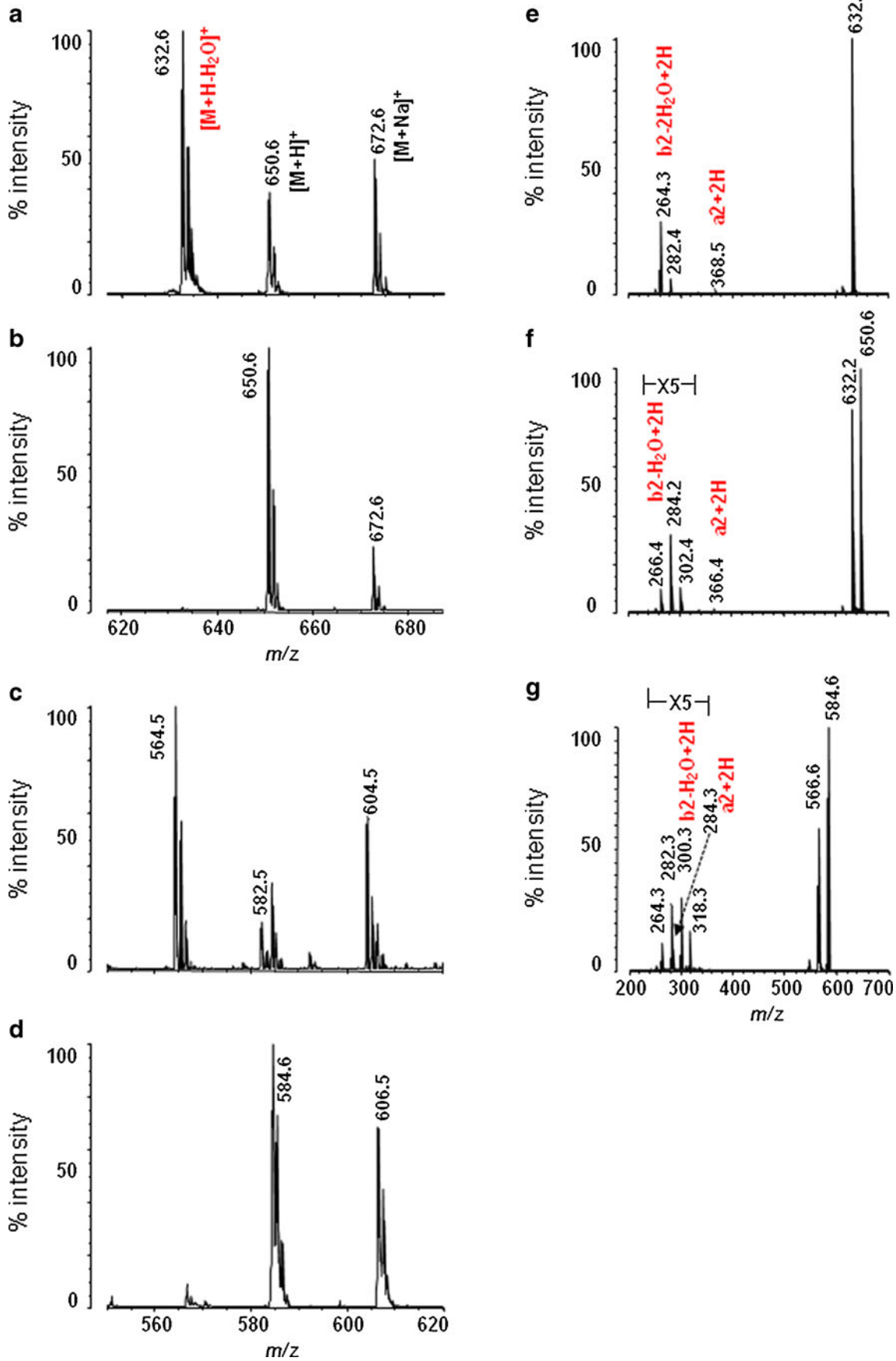
a
% intensity
100
50
0
632.6
[M+H-H2O]+
650.6
[M+H]+
672.6
[M+Na]+
b
650.6
672.6
620
640
660
680
m/z
c
564.5
582.5
604.5
d
584.6
606.5
560
580
600
620
e
632.6
b2-2H2O+2H
264.3
282.4
a2+2H
368.5
f
X5
650.6
632.2
b2-H2O+2H
284.2
266.4
302.4
366.4
g
584.6
566.6
b2-H2O+2H
284.3
a2+2H
300.3
282.3
264.3
318.3
200
300
400
500
600
700

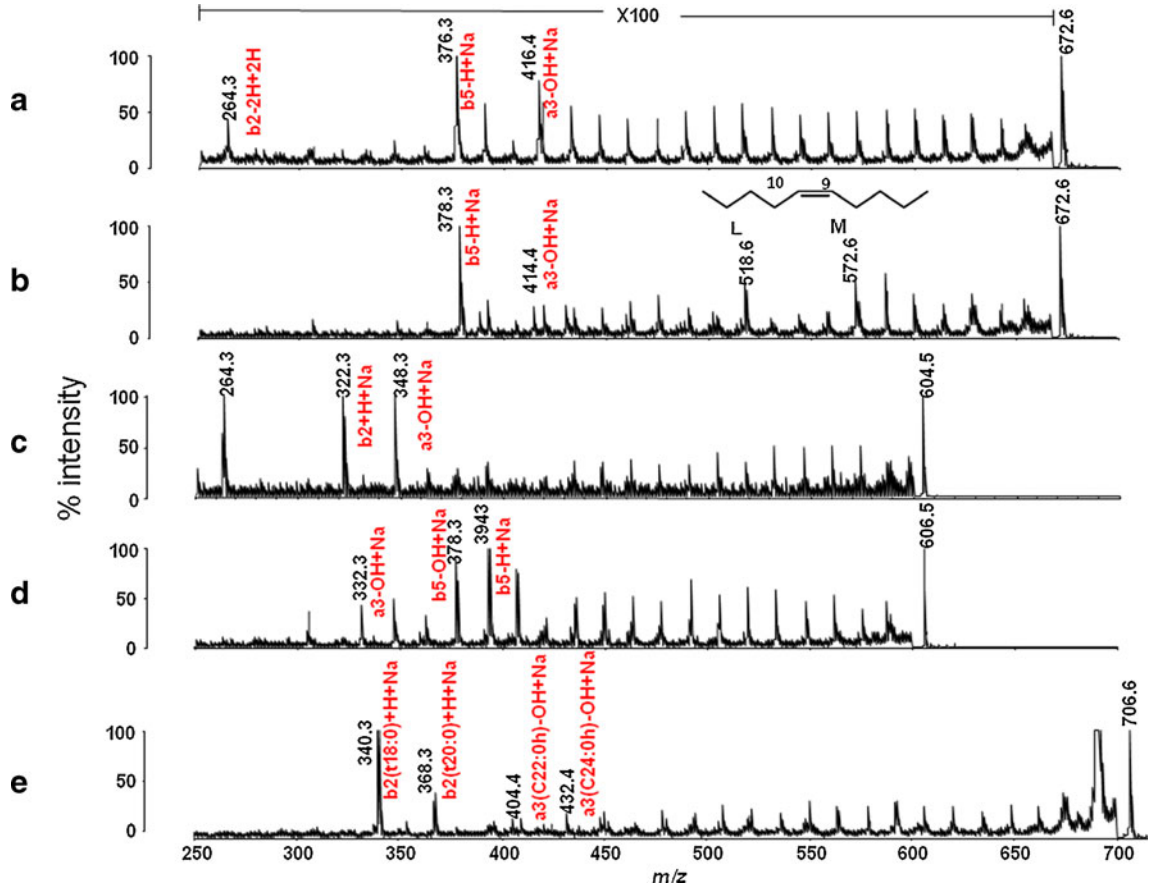

Fig. 3 MS/MS analyses of sodiated ions of the ceramides. The sodiated ion selected as the precursor was observed at *m/z* 672.6 for d18:1-C24:0 (**a**); 672.6 for d18:0-C24:1 (**b**); 604.5 for d18:1-C18:0h (**c**); 606.5 for t18:0-C18:0 (**d**) and 706.6 for t18:0-C24:0h containing a small amount of t20:0-C22:0h (**e**)

Supplemental Fig. I). The corresponding ion from d18:0-C24:1 was not observed (Fig. 3b).

To assign these fragment ions correctly, we performed MS/MS analysis of d18:1-C16:0(D31), and compared the spectra with those for d18:1-C16:0 (Fig. 4). Ions with a difference of 16 Da (-CD_2-) between ions were observed between 591.6 and at 379.6 (Fig. 4b); these were accompanied by another series of ions with a 14-Da difference between ions, indicating that the ions between 560.5 and 376.6 were derived from C16:0 and from d18:1, and that the less abundant ions in Fig. 3b between L and M were derived from d18:0. The ion at *m/z* 335.6 (a3 − OH + Na) was determined to be derived from C16:0 (D31), and the ion at 265.3 was determined to be a protonated (b2 − $2H_2O$ + H + D) ion derived from d18:1 (Fig. 4b). A hydrogen migration from the fatty acid into the LCB was previously proposed based on the analysis of *N*-acylpsychosines using FAB MS [41]. Although the efficacies of generation of product ions from fatty acids (a3 − OH + Na) were variable, that is, they were abundant among the product ions of d18:1-C16:0 (304.3) (Fig. 4a), but less abundant among those of d18:0-C24:1 (414.4) (Fig. 3b), ions derived from LCB (b5 − H + Na) were constantly prominent. The very characteristic ions derived from (b5 − H + Na) ions are specifically generated by high-energy CID and can be used as diagnostic ions for the determination of ceramide species.

Figure 3c and d show the MS/MS analyses of $[M + Na]^+$ ions derived from d18:1-C18:0h and t18:0-C18:0. In the spectrum of d18:1-C18:0h, an ion corresponding to (b5 − H + Na) was unremarkable, but an ion at *m/z* 322.3 (b2 + H + Na, an LCB of d18:1 itself) was prominent along with an ion at *m/z* 348.3 (a3 − OH + Na) derived from fatty acid (Supplemental Fig. III). The protonated ion at *m/z* 264.3 was also detected in this spectrum (Fig. 3c). On the other hand, in the spectrum for t18:0-C18:0, ions at *m/z* 394.3 (b5 − H + Na) and 332.3 (a3 − OH + Na), with an ion at *m/z* 378.3 (b5 − OH + Na), were observed (Fig. 3d and Supplemental Fig. III). Figure 3e shows the MS/MS analysis of precursor $[M + Na]^+$ at an *m/z* of 706.6 from mixtures of t18:0-C24:0h (major component) and t20:0-C22:0h (minor) from equine kidney. (b2 + H + Na) ions at *m/z* 340.3 and *m/z* 368.3 derived from t18:0 and t20:0, respectively, and (a3 − OH + Na) ions at *m/z* 404.4 and *m/z* 432.4 derived from C22:0h and C24:0h, respectively, were

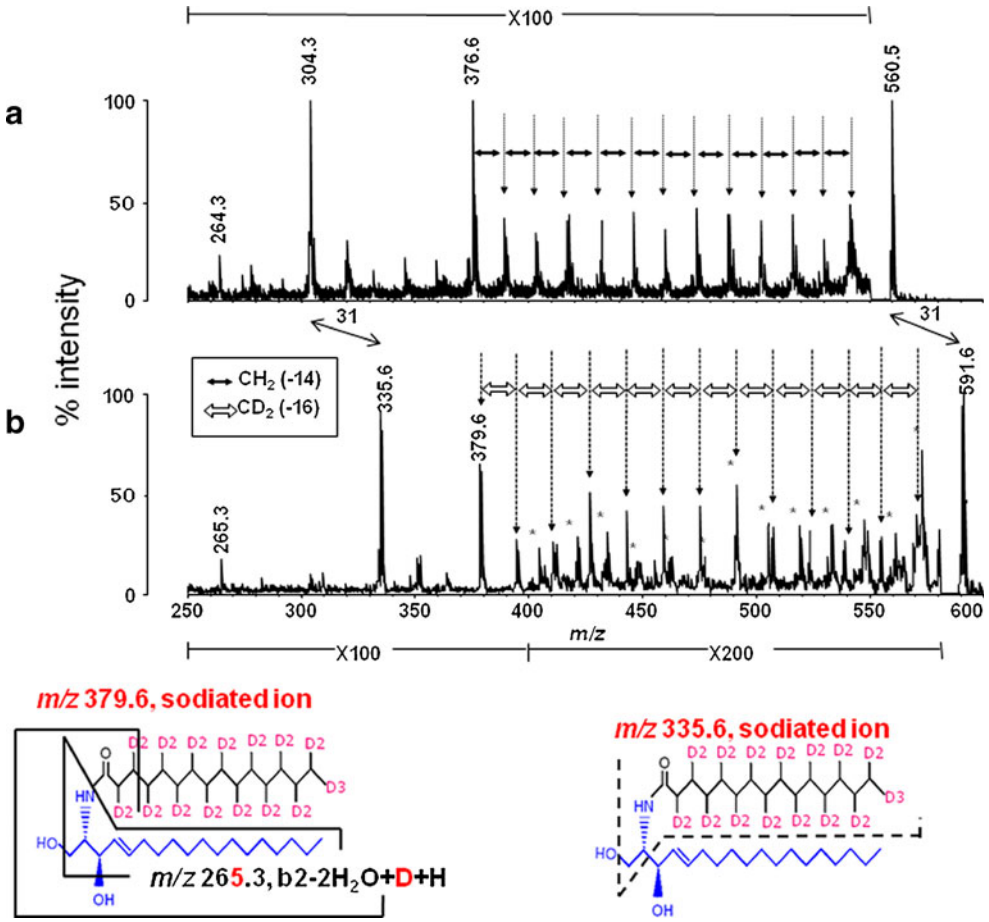

Fig. 4 MS/MS analyses of sodiated ions of the ceramide d18:1-C16:0 (**a**) and d18:1-C16:0(D31) (**b**) The asterisks indicate a series of ions with a difference of 14 Da (-CH_2-). The fragment schemes of d18:1-C16:0(D31) are drawn in the bottom row

observed (Supplemental Fig. III). The protonated ions from the LCBs were unremarkable, like those from t18:0-C18:0 (Fig. 3d). The product ions of sodiated form from various types of ceramides can be summarized as follows: i) regardless of the types of LCBs, (b5 − H + Na) ions can be used as diagnostic ions for LCB species if the ceramides contain NFAs; and ii) regardless of the types of LCBs, (b2 + H + Na) ions can be used as diagnostic ions if the ceramides contain HFAs. A protonated ion as a product ion of a sodiated precursor was probably derived from an LCB. Such an ion was observed only during the analysis of d1LCB-FA, but not during analysis of d0LCB-FA and tLCB-FA, suggesting that a trans-double bond in LCBs contributes to the generation of this ion. Although the mechanism underlying the generation of such protonated ions from sodiated precursors remains uncertain, these types of ions were also reported following an analysis of carbohydrates [42].

Linear mode and MS/MS analyses of neutral GSLs

We expanded the method to characterize GSLs. Figure 5a shows an example of a linear mode spectrum of Gb3Cers composed of d18:1-C16:0, d18:1-C22:0, d18:1-C24:1, d18:1-24:0 ,d18:1-C24:1h, and d18:1-24:0h. Corresponding $[M + Na]^+$ ions were observed at *m/z* 1046.7, 1130.8, 1156.8, 1158.8, 1172.8, and 1174.8 without dehydration of these ions. The $[M + H]^+$ ions were not observed, consistent with a previous report that, under common measurement conditions, employing DHB as a matrix, sodiated molecular $[M + Na]^+$ ions are preferentially observed in the mass spectra of neutral oligosaccharides [43]. However, from *m/z* 500 to 660, small ions were observed; these became prominent at *m/z* 520.5, 604.6, 630.6, 632.6, 646.6 and 648.6 following addition of TFA to the matrix (Fig. 5b). These ions corresponded to $(Y_0 - H_2O + 2H)^+$ ions, and were probably generated by in-source decay from $[M + H]^+$ ions of the Gb3Cers. In fact, MS/MS analyses of all $(Y_0 - H_2O + 2H)^+$ ions showed ions at *m/z* 264.3 (b2 − $2H_2O$ + 2H) (Fig. 5c), indicating that these Gb3Cers contained d18:1 as an LCB. $(Y_0 - H_2O + 2H)^+$ ions similarly correspond to $[M + H - H_2O]^+$ ions from the free ceramides containing d1LCBs (compare Fig. 2e and Fig. 5c). $[M + Na]^+$ ions of the GSLs were also subjected to MS/MS analysis. To simplify the spectra, examples of HexCer (d18:1-C24:1) and HexCer (d18:1-C18:0h) are shown in Fig. 6a and b, respectively. Ions with a difference of 14 Da between ions from *m/z* 832.7 (d18:1-C24:1) to 538.3 (Hex +

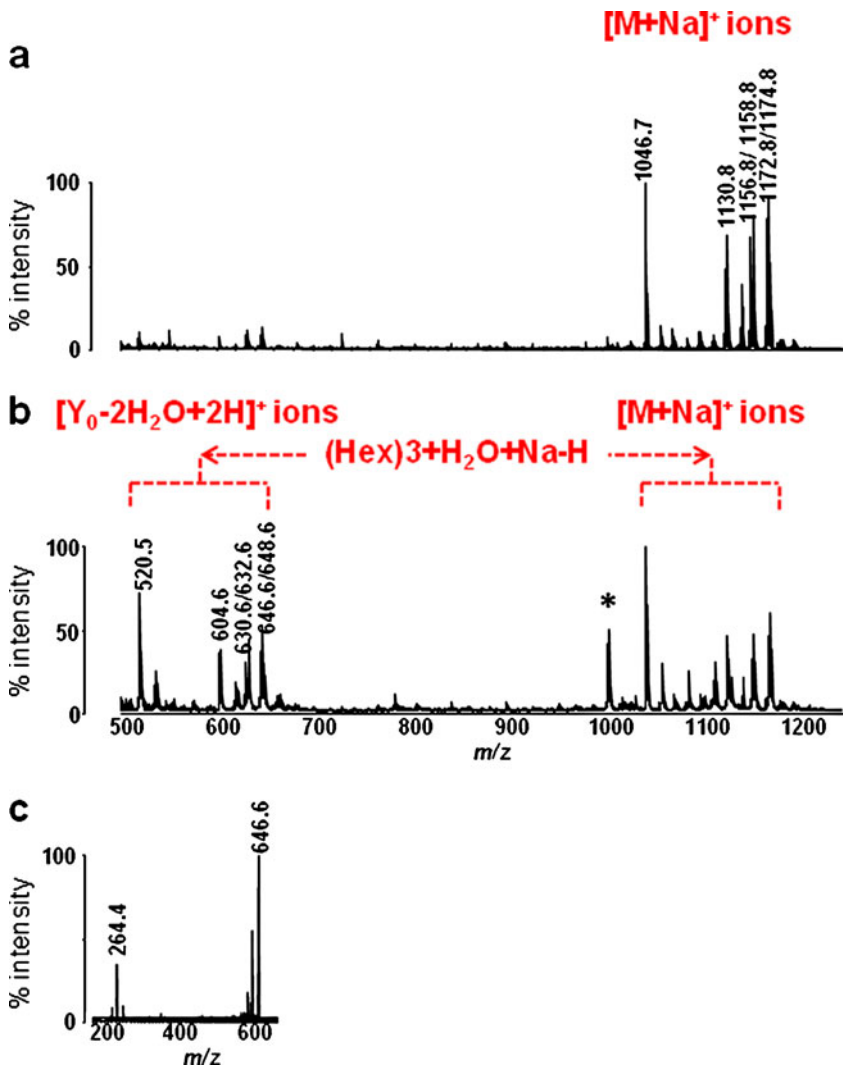

Fig. 5 Linear mode mass spectra of the authentic Gb3Cers without TFA (**a**) and with TFA (**b**). The asterisks show an unrelated peak from Gb3Cers. MS/MS analysis of the protonated ion at *m/z* 646.6 evoked with TFA(**c**)

b5 − H + Na), relatively abundant ions at *m/z* 678.6 and 732.6, indicating the occurrence of a double bond (Δ9) in C24:1, and ions at *m/z* 414.4 (a3 − H + Na), were observed along with ions at *m/z* 185.0 (B), 203.1 (C) and 244.1 (E) from Hex. In the spectra of MS/MS analysis for HexCer (d18:1-C18:0h), we observed an ion at *m/z* 484.3 (Hex + b2 + H + Na) corresponding to lysoHexCer (d18:1) and an ion at *m/z* 348.3 (a3 − OH + Na) derived from fatty acid (C18:0h) The assignments of these fragment ions were summarized in Supplemental Fig. IV.

These results indicate that the fragmentation principles observed in free ceramide analyses of both protonated and sodiated ions are directly applicable to the analysis of the molecular species of constituent ceramides in the GSLs. Thus, MS/MS analysis of a series of free ceramides and GSLs revealed that particular fragment ions can be used to

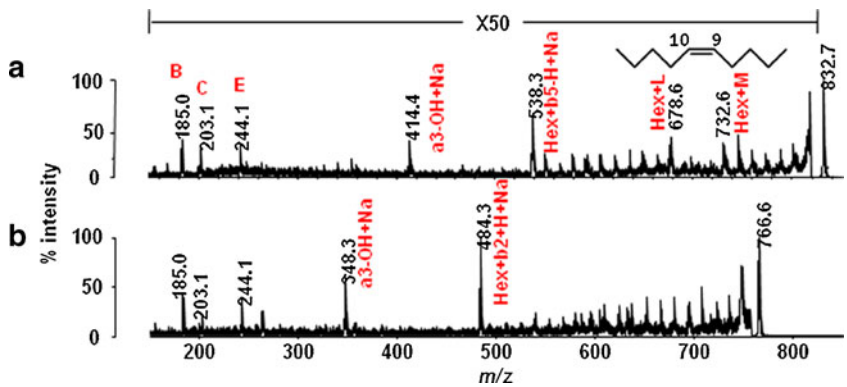

Fig. 6 MS/MS analyses of HexCer (d18:1-C24:1) at *m/z* 832.7 (**a**) and HexCer (d18:1-C18:0h) at *m/z* 766.6 (c)

define ceramide species. Namely, diagnostic ions for the LCBs can be formulated for both protonated and sodiated ions. In the case of protonated ions, regardless of the sugar chains, "b2(LCB) − $2H_2O$ + 2H" is diagnostic in cases of d1LCBs-NFAs/HFAs, and "b2(LCB) − H_2O + 2H" is diagnostic in cases of d0LCBs/tLCBs-NFA/HFA. Regarding sodiated ions, (HexNAc)n(Hex)m + b5(LCB) − H + Na is diagnostic in cases of dLCBs/tLCBs-NFAs, and (HexNAc)n(Hex)m + b2(LCB) + H + Na is diagnostic in cases of dLCBs/tLCBs-HFAs, where HexNAc and Hex are assumed to be C8H13NO5 (203.1) and C6H10O5 (162.1), respectively, and n and m are natural numbers including zero, which corresponds to cases of free ceramides. The previous finding that appearances of product ions of lysoGSLs during MS/MS analyses of GSLs possessing HFAs [20] can be expanded to free ceramides possessing HFAs. High-energy CID is indispensable for generation of (HexNAc)n(Hex)m + b5(LCB) − H + Na, but is not necessary for generation of (HexNAc)n(Hex)m + b2(LCB) + H + Na), because the appearance of such ions corresponding to lysoGSLs was reported with low-energy CID [20]. Although direct identification of fatty acid species may be practically difficult because of less generation of ions from fatty acids, they can be identified by calculating the difference in mass between the identified LCBs and the original molecules.

Linear mode and MS/MS analyses of GlcCer and GalCer from equine kidneys

We previously demonstrated diversities of free ceramides including those with NOD-LCBs from equine kidneys using ESI-MS in negative mode with low-energy CID [6]. However, this system cannot provide enough information to characterize ceramide species in GSLs; therefore, we developed the present method to identify them. Figure 7a and b shows linear mode mass spectra of GalCers and GlcCers, both of which were purified using preparative borate impregnated high-performance thin-layer chromatography, showing a clear difference. In the spectrum for GalCers, ions at *m/z* 738.5, 840.7, 854.7 and 868.7, corresponding to d18:1-C16:0h (or d18:0-C16:1h), t18:0-C22:0h, t18:0-C23:0h and t18:0-C24:0h, respectively (if simply calculated on the basis that each ion is composed of a single ceramide possessing OD-LCB), were abundant. On the other hand, in the spectrum for GlcCers, ions at *m/z* 796.6, 824.7, 838.7, and 852.7, corresponding to t18:0-C20:0, t18:0-C22:0, t18:0-C23:0, and t18:0-C24:0, respectively, were abundant. To characterize each species, MS/MS analysis was performed. Figure 8a and b show examples of MS/MS analyses of *m/z* 896.7 and 868.7 derived from GalCers. From both ions, diagnostic ions (Hex + b2 + H + Na) at *m/z* 530.4 and 502.3 were commonly detected. The ion at *m/z* 530.4 was more abundant than the ion at *m/z* 502.3 in the spectra of MS/MS analysis of the ion at *m/z* 896.7 (Fig. 8a), while the ion at *m/z* 502.3 was more abundant than the ion at *m/z* 530.4 in the spectra of MS/MS analysis of the ion at *m/z* 868.7 (Fig. 8b). An ion at 432.4 (a3 − OH + Na) was commonly detected as a product of C24:0h, but ions derived from C26:0h and C22:0h were not detected because of the limitation of sensitivity. These results indicated that the ion at *m/z* 896.7 was composed predominantly of t20:0-C24:0h, with t18:0-C26:0h as a minor component, and that the ion at *m/z* 868.7 was composed predominantly of t18:0-C24:0h, with t20:0-C22:0h as a minor component. Regardless of the use of NFAs or HFAs, the intensity of (a3 − OH + Na) ions derived from shorter chain FAs tended to be stronger than that of those ions derived from longer chain FAs. As shown in Fig. 8c, MS/MS analysis of an ion at *m/z* 766.6 revealed diagnostic ions of (Hex + b2 + H + Na) at *m/z* 456.3 and 484.3, indicating that the ion at *m/z* 766.6 was composed of d16:1-20:0h and d18:1-C18:0h. The complete results obtained for HexCers are included in Table 1. While GalCer comprised tLCB-HFAs most abundantly, followed by dLCB-HFAs, GlcCer comprised mainly tLCB-NFAs. It should be noted that usual ceramides of d18:1-NFAs are very minor and only found in GlcCer as d18:1-C16:0 and d18:1-C24:0 at *m/z* 722.6 and 834.7, respectively, as shown in Fig. 7b. HexCers containing NOD-LCBs were also detected. Namely, those commonly found in both HexCers were t20:0-C22:0h (868.7), t20:0-C24:0 (880.7), t20:0-C23:0h (882.7) and t20:0-C24:0h (896.7). Those specifically found in GalCers were d16:1-C20:0h (766.6), d20:1-C18:0h (794.6), d16:1-C23:0h (808.6) and d17:1-C23:0h (822.6), and that specifically found in GlcCers was t20:0-C25:0 (894.7).

Linear mode and MS/MS analyses of LacCer, Gb3Cer, Forssman glycolipid, and sphingomyelin from equine kidneys

Figure 7 c–f show linear mode spectra for LacCer, Gb3Cer, Forssman glycolipid, and sphingomyelin, respectively. The ions of the GSLs were sodiated and those of sphingomyelin were protonated ions. In the spectrum for LacCer (Fig. 7c), ions at *m/z* 884.6, 900.6, 984.7, 996.7, 998.7, and 1012.7, corresponding to d18:1-C16:0, d18:1-C16:0h, d18:1-C22:0h, d18:1-C24:0, d18:1-C23:0h, and d18:1-C24:0h, respectively, were abundant, indicating that the ceramide species comprising LacCer are very different from those comprising both GlcCer and GalCer. In the mass spectrum for Gb3Cer (Fig. 7d), the diversity of the ions becomes smaller and their major ions are seen at *m/z* 1046.7 (corresponding to d18:1-C16:0), 1102.7 (d18:1-C20:0), 1130.8 (d18:1-C22:0), and 1158.8 (d18:1-C24:0), with

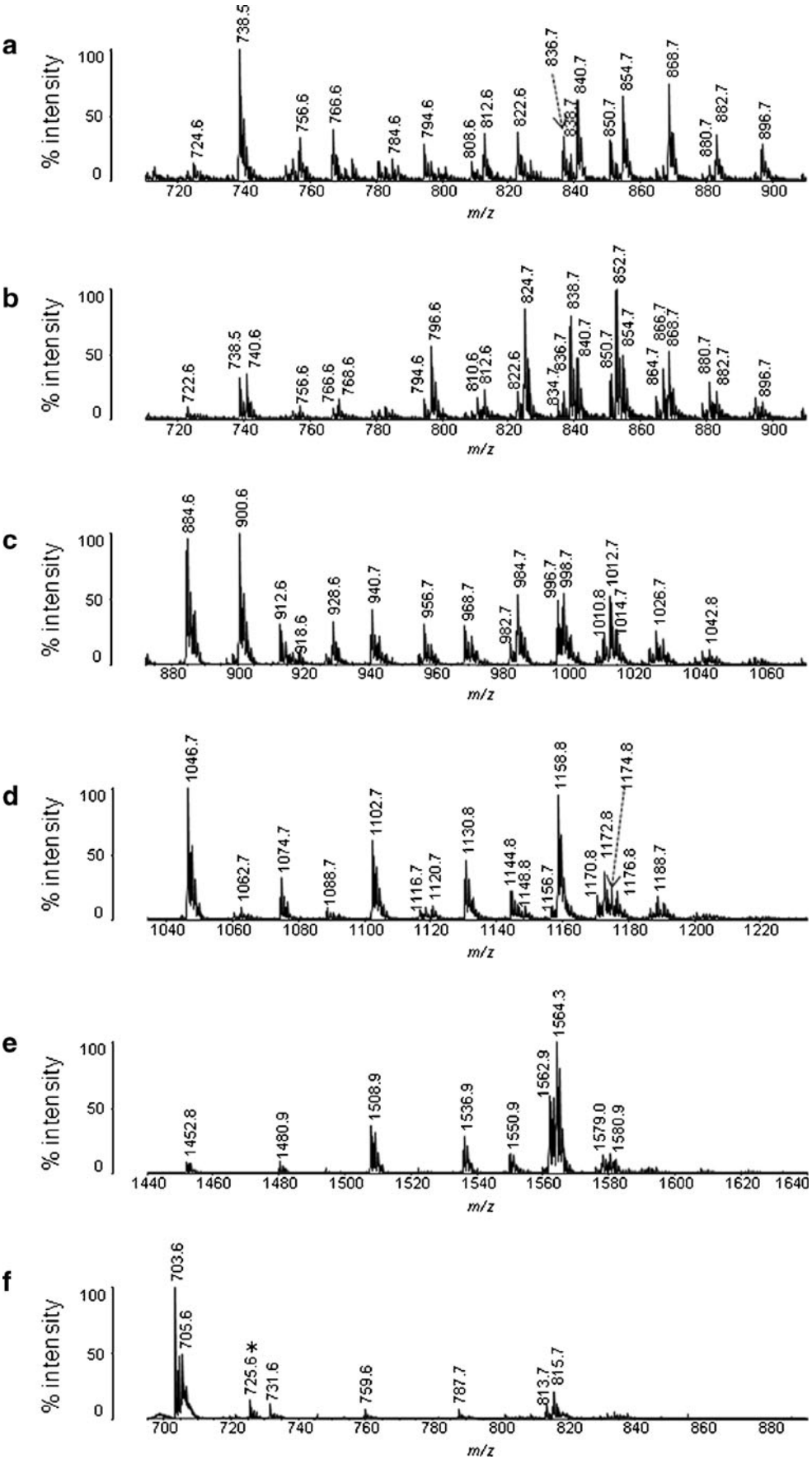

Fig. 7 Linear mode mass spectra of GalCers (**a**), GlcCers (**b**), LacCers (**c**), Gb3Cers (**d**), Forssman glycolipids (**e**), and sphingomyelins (**f**) from the equine kidneys. [M + Na] ions are found in GSLs and [M + H] ions are found in sphingomyelins. The asterisk in the spectrum for the sphingomyelins is $[M + Na]^+$ (**f**). By calculating the difference in molecular weight between each polar head-group of the sphingolipid, the spectra were displayed to compare each peak directly, if simply calculated each ion as composed of a single ceramide possessing an OD-LCB

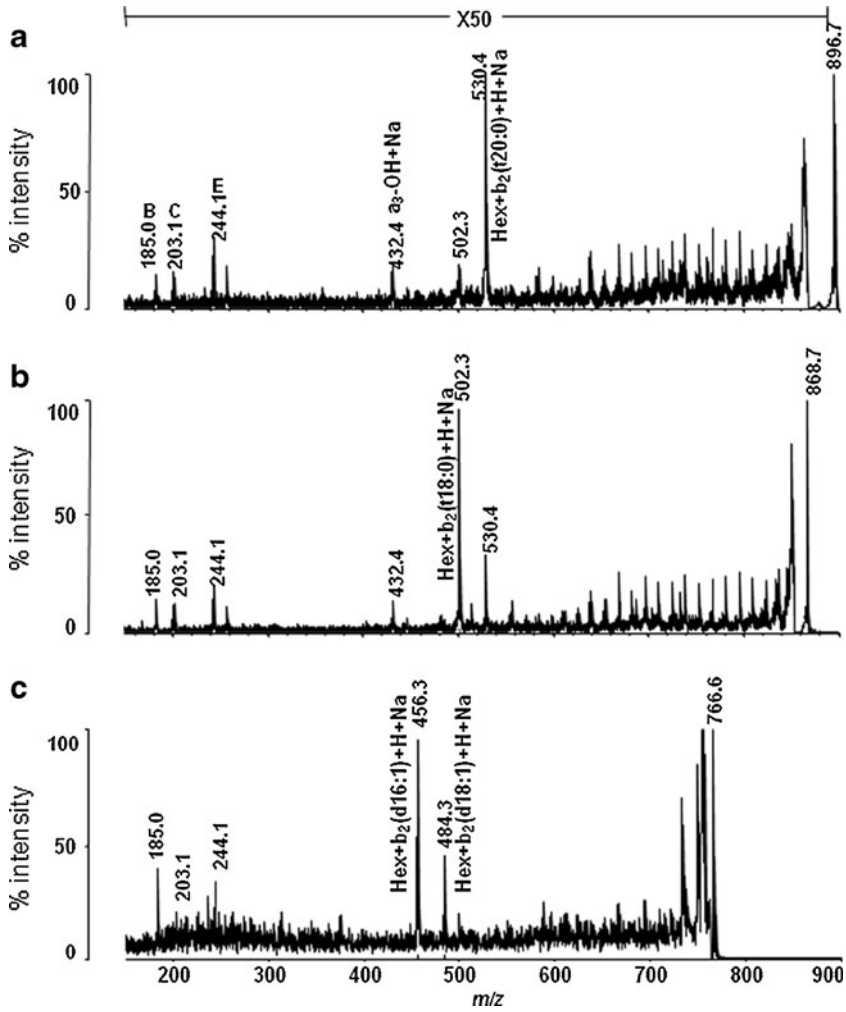

Fig. 8 MS/MS analyses of the GalCers at *m/z* 896.7 (**a**), 868.7 (**b**) and 766.6 (**c**). The ion at *m/z* 868.7 was predominantly composed of t18:0-C24:0h with t20:0-C22:0h as a minor component; the ion at *m/z* 896.7 was predominantly t20:0-C24:0h with t18:0-C26:0h as a minor component; and the ion at *m/z* 766.6 was predominantly d16:1-20:0h with d18:1-C18:0h as a minor component

some minor ions at *m/z* 1174.8 (d18:1-C24:0h) and 1176.8 (t18:0-C24:0) that are major types of ions in the spectra for HexCers (Fig. 7a and b). In the spectrum for Forssman glycolipid (Fig. 7e), this trend becomes more obvious and major ions are seen at *m/z* 1508.9 (d18:1-C20:0), 1536.9 (d18:1-C22:0), 1564.3 (d18:1-C24:0) and 1562.9 (d18:1-C24:1), the latter type of which was hardly observed in spectra for HexCers to Gb3Cer. A similar linear mode spectra pattern to that of Forssman glycolipid was observed in the spectra for Gb4Cer (data not shown). The sphingomyelin mass spectrum pattern was very different from those for all GSLs (Fig. 7f), and an ion at *m/z* 703.6 corresponding to d18:1-C16:0 was dominant.

To confirm the ceramide species comprising these GSLs, MS/MS analysis was performed using protonated ions evoked by adding TFA to the matrix. Ceramide species derived from sphingomyelin were analyzed as ceramides after being digested with sphingomyelinase. Table 2 summarizes the results, in which ($Y_0 - H_2O + 2H$) presents diagnostic ions of LCBs for GSLs and Cer − H_2O + H does the same for sphingomyelin.

For some GSLs, $[M + Na]^+$ ions were directly analyzed by MS/MS together with MS/MS analysis of protonated ions evoked by TFA. Figure 9a shows MS/MS analyses of the protonated ion ($Y_0 - H_2O + 2H$) evoked by TFA at *m/z* 565.6 (left) and the $[M + Na]^+$ ion at *m/z* 928.6 (right) derived from LacCers. From the protonated ion, product ions at *m/z* 236.7 [b2(d16:1) − $2H_2O$ + 2H] and 264.3 [b2(d18:1) − $2H_2O$ + 2H] were detected. Accordingly, from the $[M + Na]^+$ ion at *m/z* 928.6, ions at *m/z* 618.3 [Hex2 + b2(d16:1) + H + Na] and 646.4 [Hex2 + b2(d18:1) + H + Na] were observed. Both results consistently showed the ion at *m/z* 928.6 derived from Hex2Cer to be composed of d18:1-C18:0h and d16:1-C20:0h.

In the spectrum for Gb3Cer (Fig. 7d), an ion at *m/z* 1172.8 was observed. The protonated ion of ($Y_0 - H_2O$ + 2H) generated at *m/z* 646.6 from this species was analyzed by MS/MS, and an ion at *m/z* 264.3 was observed (data not shown), indicating this species has d18:1 as an LCB. However, the result still cannot discriminate Gb3Cer having either d18:1-C24:1h (C60H111NO19Na, 1172.8) or d18:1-C25:0 (C61H115NO18Na, 1172.8). The ions at *m/z* 1172.8

Table 1 Identified sodiated ions from GalCer, ClcCer and LacCer

Species	GalCer			GlcCer			LacCer		
	M + Na	b5 − H + Na	b2 + H + Na	M + Na	b5 − H + Na	b2 + H + Na	M + Na	b5 − H + Na	b2 + H + Na
d18:1-C16:0	-	-	-	722.6	538.3	-	884.6	700.4	-
d18:0-C16:0	724.6	540.4	-	-	-	-	-	-	-
d18:1-C16:0h	738.5	-	484.3	738.5	-	484.3	900.6	-	646.4
t18:0-C16:0	-	-	-	740.6	556.3	-	-	-	-
d16:1-C20:0	-	-	-	-	-	-	912.6	672.4	-
d18:1-C18:0	-	-	-	-	-	-	912.6	700.4	-
t18:0-C16:0h	756.6	-	502.3	756.6	-	502.3	918.6	-	664.4
d16:1-C20:0h	766.6	-	456.3	766.6	-	456.3	928.6	-	618.4
d18:1-C18:0h	766.6	-	484.3	766.6	-	484.3	928.6	-	646.4
t18:0-C18:0	-	-	-	768.6	556.3	-	-	-	-
d16:1-C22:0	-	-	-	-	-	-	940.7		-
d18:1-C20:0	-	-	-	-	-	-	940.7	700.4	-
t18:0-C18:0h	784.6	-	502.3	-	-	-	-	-	-
d16:1-C22:0h	-	-	-	-	-	-	956.7	-	618.4
d18:1-C20:0h	794.6	-	484.3	794.6	-	484.3	956.7	-	646.4
t18:0-C20:0	-	-	-	796.6	556.3	-	-	-	-
d18:1-C22:0	-	-	-	-	-	-	968.7	700.4	-
d16:1-C23:0h	808.6	-	456.3	-	-	-	-	-	-
d18:1-C21:0h	808.6	-	484.3	-	-	-	-	-	-
t18:0-C21:0	-	-	-	810.6	556.3	-	-	-	-
t18:0-C20:0h	812:6	-	502.3	812.6	-	502.3	-	-	-
d18:1-C23:0	-	-	-	-	-	-	982.7	*	-
d17:1-C23:0h	822.6	-	470.3	-	-	-	-	-	-
d18:1-C22:0h	822.6	-	484.3	822.6	-	484.3	984.7	-	646.4
t18:0-C22:0	-	-	-	824.7	556.3	-	-	-	-
d18:1-C24:0	-	-	-	834.7	538.3	-	996.7	700.4	-
d18:1-C23:0h	836.7	-	484.3	836.7	-	484.3	998.7	-	646.4
t18:0-C23:0	838.7	556.3	-	838.7	556.3	-	-	-	-
t18:0-C22:0h	840.7	-	502.3	840.7	-	502.3	-	-	-
d18:1-C25:0	-	-	-	-	-	-	1010.8	700.4	-
d18:1-C24:0h	850.7	-	484.3	850.7	-	484.3	1012.7	-	646.4
t18:0-C24:0	-	-	-	852.7	556.3	-	1014.7	-	-
t20:0-C22:0	-	-	-	-	-	-	1014.7	*	-
t18:0-C23:0h	854.7	-	502.3	854.7	-	502.3	-	-	-
d18:1-C25:0h	-	-	-	864.7	-	484.3	1026.7	-	646.4
t18:0-C25:0	-	-	-	866.7	556.3	-	-	-	-
t18:0-C24:0h	868.7	-	502.3	868.7	-	502.3	-	-	-
t20:0-C22:0h	868.7	-	530.4	868.7	-	530.4	-	-	-
d18:1-C26:0h	-	-	-	878.7	-	-	-	-	-
t18:0-26:0	880.7	556.3	-	880.7	556.3	-	1042.8	*	-
t20:0-C24:0	880.7	584.4	-	880.7	584.4	-	1042.8	*	-
t18:0-C25:0h	882.7	-	502.3	882.7	-	502.3	-	-	-
t20:0-C23:0h	882.7	-	530.4	882.7	-	530.4	-	-	-
t18:0-C26:0h	896.7	-	502.3	896.7	-	502.3	-	-	-
t20:0-C24:0h	896.7	-	530.4	896.7	-	530.4	-	-	-

- not dectected, * not detected but the species were confirmed as protonated ions, see Table 2

Table 2 Identified ions from LacCer, Gb3Cer, Forssman glycolipid and sphingomyelin

Species	LacCer					Gb3Cer					Forssman glycolipid					Sphingomyelin				
	M + Na	$Y_0 - H_2O + 2H$	$Y_0 + 2H$	b2 $- 2H_2O + 2H$	b2 $- H_2O + 2H$	M + Na	$Y_0 - H_2O + 2H$	$Y_0 + 2H$	b2 $- 2H_2O + 2H$	b2 $- H_2O + 2H$	M + Na	$Y_0 - H_2O + 2H$	$Y_0 + 2H$	b2 $- 2H_2O + 2H$	b2 $- H_2O + 2H$	M + H	Cer* $- H_2O + H$	Cer* + H	b2 $- 2H_2O + 2H$	b2 $- H_2O + 2H$
d18:1-C16:0	884.6	520.5	-	264.3	-	1046.7	520.5		264.3	-	1452.8	520.5	-	264.3	-	703.6	520.5	-	264.3	-
d16:0-C18:0	-	-	-	-	-	-	-	-	-	-	-	-	-	-	-	705.6	-	540.5	-	256.3
d18:0-C16:0	-	-	-	-	-	-	-	-	-	-	-	-	-	-	-	705.6	-	540.5	-	284.3
d18:1-C16:0h	900.6	536.5	-	264.3	-	1062.7	536.5	-	264.3	-	-	-	-	-	-	-	-	-	-	-
d16:1-C20:0	912.6	548.5	-	236.2	-	1074.7	548.5	-	236.2	-	-	-	-	-	-	731.6	548.5	-	236.2	-
d18:1-C18:0	912.6	548.5	-	264.3	-	1074.7	548.5	-	264.3	-	1480.9	548.5	-	264.3	-	731.6	548.5	-	264.3	-
t18:0-C16:0h	918.6	-	572.5	-	300.3	-	-	-	-	-	-	-	-	-	-	-	-	-	-	-
d16:1-C21:0	-	-	-	-	-	1088.7	562.5	-	236.2	-	-	-	-	-	-	-	-	-	-	-
d17:1-C20:0	-	-	-	-	-	1088.7	562.5	-	250.3	-	-	-	-	-	-	-	-	-	-	-
d18:1-C19:0	-	-	-	-	-	1088.7	562.5	-	264.3	-	-	-	-	-	-	-	-	-	-	-
d16:1-C20:0h	928.6	564.5	-	236.2	-	-	-	-	-	-	-	-	-	-	-	-	-	-	-	-
d18:1-C18:0h	928.6	564.5	-	264.3	-	-	-	-	-	-	-	-	-	-	-	-	-	-	-	-
d16:1-C22:0	940.7	576.6	-	236.2	-	-	-	-	-	-	-	-	-	-	-	-	-	-	-	-
d18:1-C20:0	940.7	576.6	-	264.3.	-	1102.7	576.6	-	264.3	-	1508.9	576.6	-	264.3	-	759.6	576.6	-	264.3	-
d17:1-C22:0	-	-	-	-	-	1116.7	590.6	-	250.3	-	-	-	-	-	-	-	-	-	-	-
d18:1-C21:0	-	-	-	-	-	1116.7	590.6	-	264.3	-	-	-	-	-	-	-	-	-	-	-
t18:0-C20:0	-	-	-	-	-	1120.7	-	612.6	-	300.3	-	-	-	-	-	-	-	-	-	-
d16:1-C22:0h	956.7	592.6	-	236.2	-	-	-	-	-	-	-	-	-	-	-	-	-	-	-	-
d18:1-C20:0h	956.7	592.6	-	264.3	-	-	-	-	-	-	-	-	-	-	-	-	-	-	-	-
d18:1-C22:0	968.7	604.6	-	264.3	-	1130.8	604.6	-	264.3	-	1536.9	604.6	-	264.3	-	787.7	604.6	-	264.3	-
d17:1-C24:0	-	-	-	-	-	1144.8	618.6	-	250.3	-	-	-	-	-	-	-	-	-	-	-
d18:1-C23:0	982.7	618.6	-	264.3	-	1144.8	618.6	-	264.3-	-	1550.9	618.6	-	264.3	-	-	-	-	-	-
d18:1-C22:0h	984.7	620.6	-	264.3	-	-	-	-	-	-	-	-	-	-	-	-	-	-	-	-
t18:0-C22:0	-	-	-	-	-	1148.8	-	640.6	-	300.3	-	-	-	-	-	-	-	-	-	-

Table 2 (continued)

Species	LacCer					Gb3Cer					Forssman glycolipid					Sphingomyelin				
	M + Na	$Y_0 - H_2O + 2H$	$Y_0 + 2H$	$b2 - 2H_2O + 2H$	$b2 - H_2O + 2H$	M + Na	$Y_0 - H_2O + 2H$	$Y_0 + 2H$	$b2 - 2H_2O + 2H$	$b2 - H_2O + 2H$	M + Na	$Y_0 - H_2O + 2H$	$Y_0 + 2H$	$b2 - 2H_2O + 2H$	$b2 - H_2O + 2H$	M + H	Cer* $- H_2O + H$	Cer* + H	$b2 - 2H_2O + 2H$	$b2 - H_2O + 2H$
d18:1-C24:1	-	-	-	-	-	1156.8	630.6	-	264.3	-	1562.9	630.6	-	264.3	-	813.7	630.6	-	264.3	-
d18:1-C24:0	996.7	632.6	-	264.3	-	1158.8	632.6	-	264.3	-	1564.9	632.6	-	264.3	-	815.7	632.6	-	264.3	-
d18:1-C23:0h	998.7	634.6	-	264.3	-	-	-	-	-	-	-	-	-	-	-	-	-	-	-	-
d18:1-C25:1	-	-	-	-	-	1170.8	644.6	-	264.3	-	-	-	-	-	-	-	-	-	-	-
d18:1-C25:0	1010.8	646.7	-	264.3	-	1172.8	646.7	-	264.3	-	1579.0	646.7	-	264.3	-	-	-	-	-	-
d18:1-C24:0h	1012.7	648.6	-	264.3	-	1174.8	648.7	-	264.3	-	1580.9	648.6	-	264.3	-	-	-	-	-	-
t18:0-C24:0	1014.7	-	668.7	-	300.3	1176.8	-	668.7	-	300.3	-	-	-	-	-	-	-	-	-	-
t20:0-C22:0	1014.7	-	668.7	-	328.3	-	-	-	-	-	-	-	-	-	-	-	-	-	-	-
d18:1-C25:0h	1026.7	662.6	-	264.3	-	1188.8	662.7	-	264.3	-	-	-	-	-	-	-	-	-	-	-
t18:0-C26:0	1042.8	-	696.7	-	300.3	-	-	-	-	-	-	-	-	-	-	-	-	-	-	-
t20:0-C24:0	1042.8	-	696.7	-	328.3	-	-	-	-	-	-	-	-	-	-	-	-	-	-	-

-not detected, *species were analyzed as free ceramides after treatment with sphingomyelinase

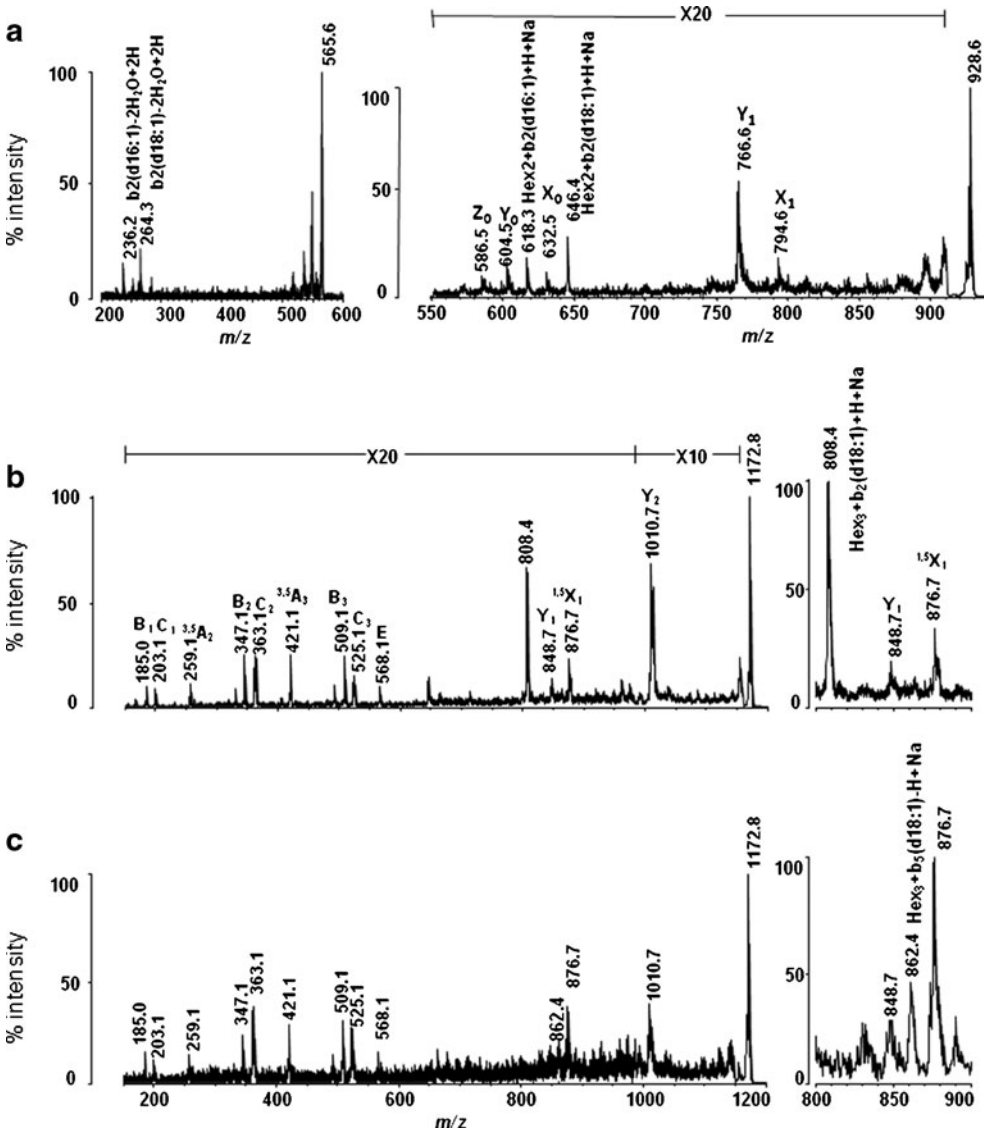

Fig. 9 MS/MS analyses of LacCer and Gb3Cers. The spectra for the protonated ion at *m/z* 565.6 evoked with TFA (*left*) and the $[M + Na]^+$ ion at *m/z* 928.6 (*right*) from the LacCers, consistently indicating that the $[M + Na]^+$ at *m/z* 928.6 was composed of LacCer d18:1-C16:0h and d16:1-C18:0h (**a**). MS/MS spectra for the isobaric ions at *m/z* 1172.8 from the Gb3Cer d18:1-C24:1h from porcine erythrocytes (**b**) and Gb3Cer d18:1-C25:0 from the kidneys (**c**). The ion at *m/z* 808.4 was observed in the spectra for d18:1-C24:1h, but not in the spectra for d18:1-C25:0. Instead, the ion at *m/z* 862.4 was observed in the spectra from d18:1-C25:0 (right panels in b and c). The ion at *m/z* 259.1 ($^{3,5}A_2$), indicating a Hex1-4Hex linkage, revealed both Hex3Cers as Gb3Cers, but not iGb3Cers

in the authentic Gb3Cer possessing d18:1-C24:1h derived from porcine erythrocytes and in this Gb3Cer were comparatively analyzed by MS/MS (Fig. 9 b and c, also see Fig. 5). Among commonly found A, B, C series ions from Hex-Hex-Hex, an ion at *m/z* 259.1 ($^{3,5}A_2$), indicating Hex1-4Hex linkage, determined both Hex3Cers as Gb3Cers, but not iGb3Cers [1]. In addition to these sugar-derived ions, in the authentic spectrum, a prominent ion at *m/z* 808.4 [Hex3 + b2(d18:1) + H + Na] was detected (Fig. 9b). On the other hand, in the spectrum for Gb3Cer from equine kidney, the ion at *m/z* 808.4 was not observed. Instead, a small but definite ion at *m/z* 862.4 was observed as [Hex3 + b5(d18:1) − H + Na] (Fig. 9c see right panel), indicating that the ion at *m/z* 1172.8 was derived from Gb3Cer with d18:1-C25:0. Therefore, MS/MS analysis of protonated ions evoked by TFA in the matrix is informative for discriminating between ceramide species. However, for isobaric cases, MS/MS analysis of $[M + Na]^+$ ions is effective for discriminating between species, although [(Hex)n(HexNAc)m + b2 + H + Na] and [(Hex)n(HexNAc)m + b5 − H + Na] ions become smaller, especially in the cases of the latter ions derived from GSLs with longer sugar chains.

Figure 10 a shows the results of MS/MS analysis of the $[M + Na]^+$ ion at *m/z* 1562.9 from Forssman glycolipid. Two series of ions from the sugar sequences of HexNAc-HexNAc-Hex-Hex-Hex were identified at 226.1 (B_1), 244.1 (C_1), 429.1 (B_2), 445.1 (C_2), 591.2 (B_3), 607.1 (C_3), 665.2 ($^{3,5}A_4$), 753.2 (B_4), 769.2 (C_4) 827.3 ($^{3,5}A_5$), 915.3 (B_5), and 931.3 (C_5); and at 1184.8 (X_3), 1156.8 (Y_3), 1022.8 (X_2) and 994.7 (Y_2). In addition, although they are small, the ion at *m/z* 1268.6 [b5(d18:1) − H + Na] continuous ions with a 14-Da difference including the ions indicating the occurrence of a double bond $\Delta 9$ in C24:1, and Y_4 (1359.8)

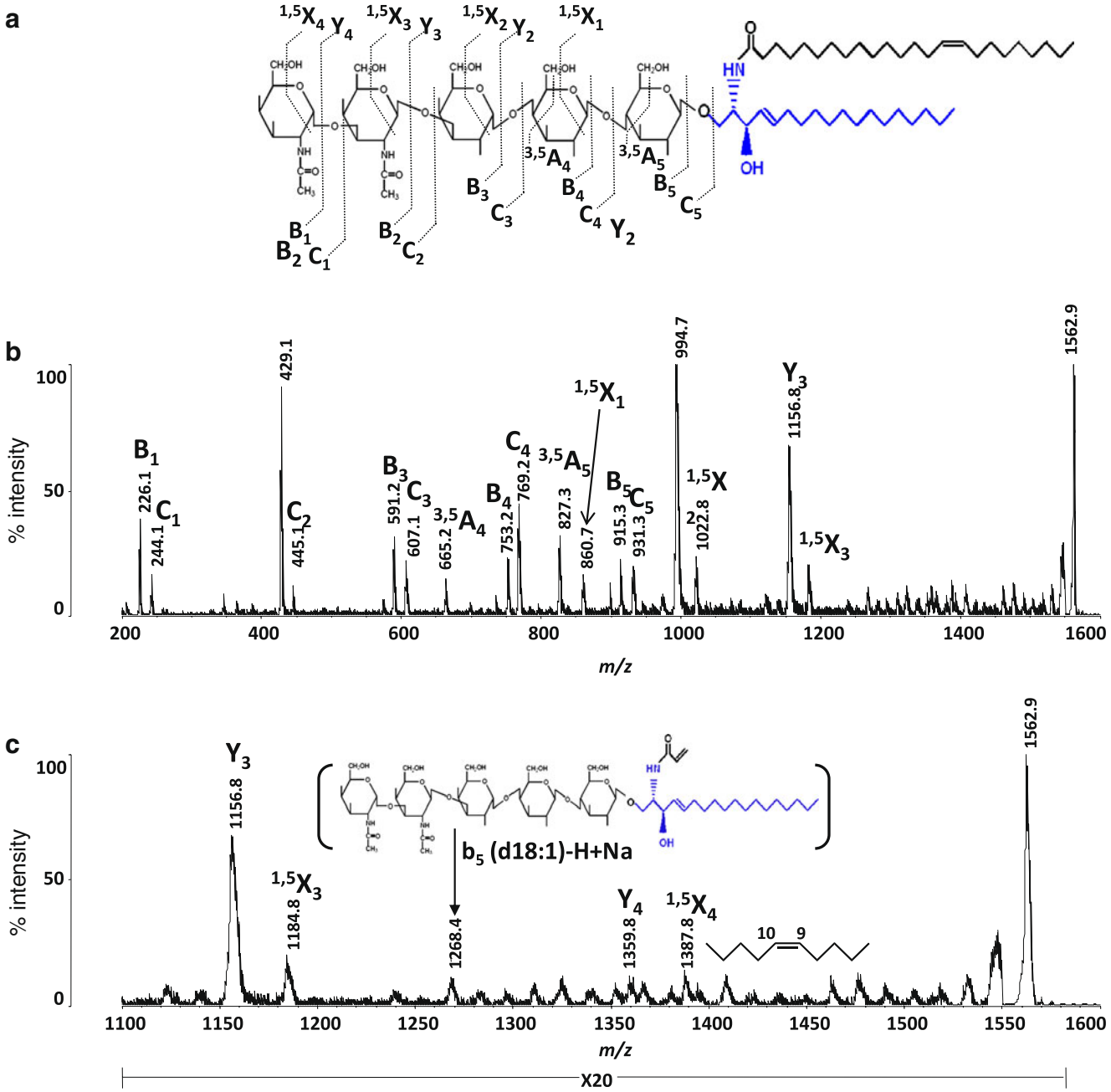

Fig. 10 Fragmentation scheme (**a**) and whole MS/MS profile of the $[M + Na]^+$ ion at *m/z* 1562.9 derived from Forssman glycolipid with d18:1-C24:1 (**b**) and its enlargement spectrum, showing the ion at *m/z* 1268.6 [b5(d18:1) − H + Na], continuous ions with a 14-Da difference including three skips, Y_4 (1360.4) and $^{1,5}X_4$ (1387.4)

and $^{1,5}X_4$ (1387.8), are clearly observed. Furthermore, by adding TFA to the matrix, a protonated ion at 630.6 ($Y_0 - H_2O + 2H$) was observed, from which an ion at *m/z* 264.3 ($b1 - 2H_2O + 2H$) was produced by MS/MS analysis (data not shown). Collectively these product ions definitely indicate that the ion at *m/z* 1562.9 comprises Forssman glycolipid whose ceramide portion is composed of d18:1-C24:1. The composed ceramides in sphingomyelin were analyzed as free ceramides after sphingomyelinase treatment. The results indicated that the ion at *m/z* 705.6 was composed of d16:0-C18:0 and d18:0-C16:0, and that the ion at *m/z* 731.6 was composed of d16:1-C20:0 and d18:1-C18:0.

Fig. 11 Ceramide compositions of the free ceramides, sphingomyelin and GSLs from equine kidneys. Compositions were calculated based on the peak areas of linear mass spectra. Each column represents a single ceramide with an OD-LCB, and the asterisks above the columns indicate additional numbers of isomers with NOD-LCBs

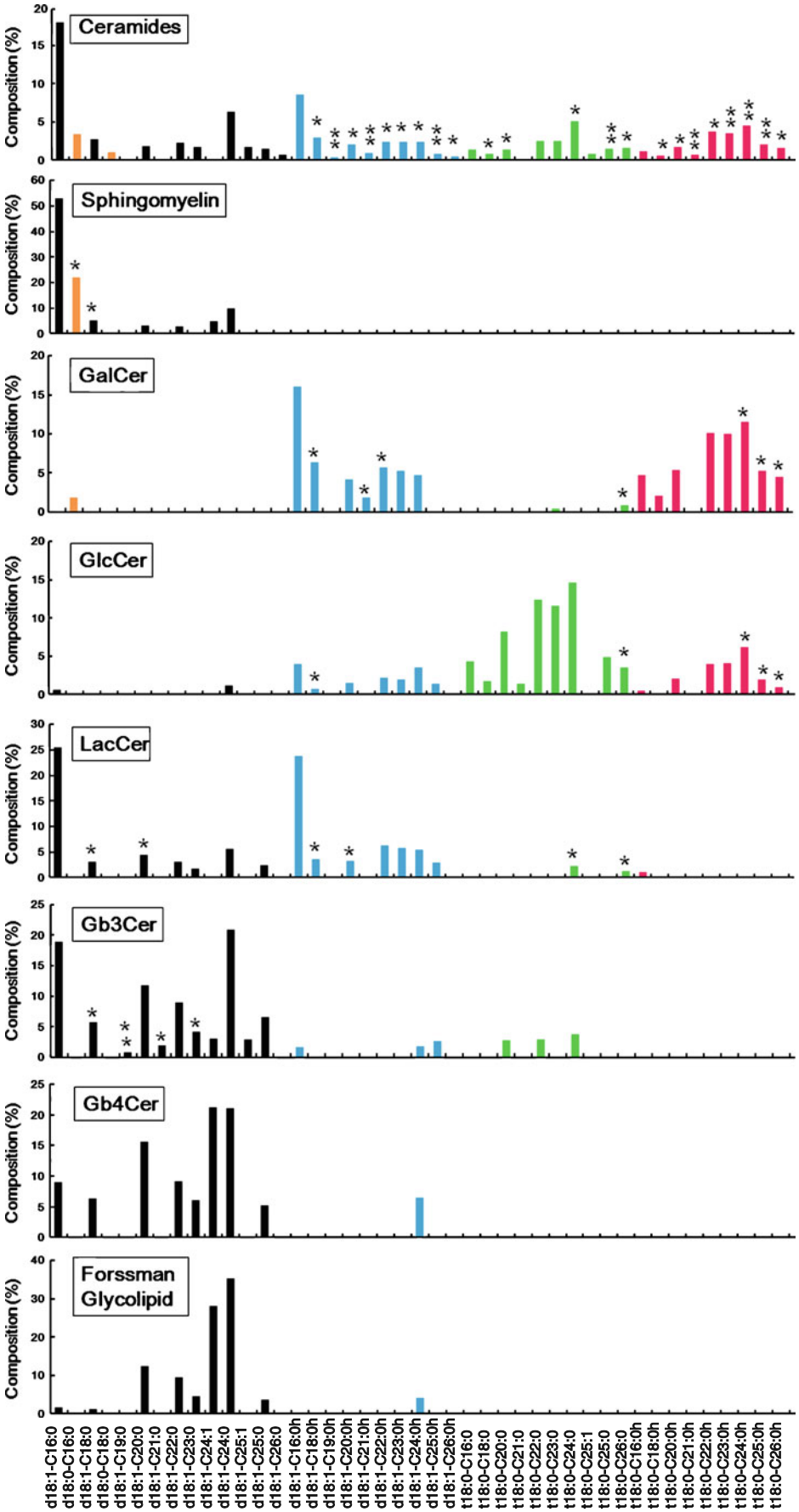
Ceramides
Sphingomyelin
GalCer
GlcCer
LacCer
Gb3Cer
Gb4Cer
Forssman Glycolipid
Composition (%)
d18:1-C16:0
d18:0-C16:0
d18:1-C18:0
d18:0-C18:0
d18:1-C19:0
d18:1-C20:0
d18:1-C21:0
d18:1-C22:0
d18:1-C23:0
d18:1-C24:1
d18:1-C24:0
d18:1-C25:1
d18:1-C25:0
d18:1-C26:0
d18:1-C16:0h
d18:1-C18:0h
d18:1-C19:0h
d18:1-C20:0h
d18:1-C21:0h
d18:1-C22:0h
d18:1-C23:0h
d18:1-C24:0h
d18:1-C25:0h
d18:1-C26:0h
t18:0-C16:0
t18:0-C18:0
t18:0-C20:0
t18:0-C21:0
t18:0-C22:0
t18:0-C23:0
t18:0-C24:0
t18:0-C25:1
t18:0-C25:0
t18:0-C26:0
t18:0-C16:0h
t18:0-C18:0h
t18:0-C20:0h
t18:0-C21:0h
t18:0-C22:0h
t18:0-C23:0h
t18:0-C24:0h
t18:0-C25:0h
t18:0-C26:0h

Compositional comparison of the ceramides species among the free ceramides, sphingomyelins, GalCers, GlcCers, LacCers, Gb3Cers, Gb4Cers and Forssman glycolipids in the equine kidneys

Figure 11 summarizes the ceramide compositions of the free ceramides, sphingomyelin and GSLs from equine kidneys. The free ceramides previously analyzed by ESI [5] were re-analyzed using this MALDI-TOF MS, resulting in the similar outcomes (data not shown). These compositions were tentatively calculated based on the peak areas of the linear mass spectra. We compared the FA compositions of the authentic Cers and GalCers containing NFAs and HFAs determined by conventional gas-liquid chromatography and by peak area calculation based on the MALDI-TOF MS results. Because these results showed similar trends (personal communication), the ionization potentials of sphingolipids with HFAs and NFAs might be similar, although the exact potential of each class of lipid should be examined in the future. To avoid expanding the figure, each column represents a single ceramide with OD-LCB, and the asterisks above the columns indicate additional numbers of isomers with NOD-LCBs. Free ceramides are the most diverse group (total 69), comprising dLCB-NFAs (11, no ceramides with NOD-LCBs), dLCB-HFAs (22, including 12 ceramides with NOD-LCBs), tLCB-NFAs (15, including 6 ceramides with NOD-LCBs) and tLCB-HFAs (21, including 12 ceramides with NOD-LCBs). The NOD-LCBs in the free ceramides are d16:1/t16:0, d17:1/t17:0, d19:1/t19:0 and d20:1/t20:0 and the ceramides with NOD-LCBs tended to contain FAs with longer acyl chains, but contained neither palmitate (C16:0) nor its hydroxylated form C16:0h as previously reported [6]. The sphingomyelins were composed of nine species that contained dLCB-NFAs only without dLCB-HFAs, tLCB-NFAs/HFAs. Although NOD-LCBs were not found in the dLCB-NFAs of the free ceramides, these were detected as d16:0-C18:0 and d16:1-C20:0 in the sphingomyelins. The species with d18:1-C24:1, which was not found among the free ceramides, was detected in the sphingomyelins. On the other hand GalCers are composed of 25 species (including six ceramides with NOD-LCBs as d16:1, d17:1 and t20:0) and their major species are ceramides possessing HFAs with dLCB or tLCB. The major HFA combined with dLCB was C16:0h, while that with tLCB was a very long acyl chain of C24:0h. GlcCers are composed of 30 species including five ceramides with NOD-LCBs (d16:1 and t20:0). Their major ceramides species are the so-called hydroxyl-ceramides [6], tLCB-NFAs/HFAs and dLCB-HFAs, but dLCB-NFAs were minor. These results suggest characteristic preferences of sphingomyelins, GalCers and GlcCers for employing their constituent ceramides. Ceramides are synthesized at the cytosolic surface of the endoplasmic reticulum through condensation of L-serine palmitoyl-CoA (at least OD-LCBs), reduction, acylation, and/or desaturation [1]. Some of them are hydroxylated to become tLCB-NFAs/HFAs. These processes produce diversity among the ceramide species found in the free ceramides. Nevertheless, the sphingomyelins in the equine kidneys persistently employed dLCB-NFAs only, suggesting some preference, although, there have been several reports of the presence of HFAs and/or tLCBs in sphingomyelins from bovine kidneys [44, 45], rennet stomach [46] and intestinal mucosa [45], murine epidermis [47] and the testes and spermatozoa of various animals [48]. The results observed in the GalCers are consistent with previous reports that ceramide galactosyltransferase in the endoplasmic reticulum prefers ceramides possessing HFAs as substrates to those possessing NFAs [49, 50].

LacCers were composed of 23 species including six ceramides with NOD-LCBs (d16:1 and t20:0). In contrast to GlcCers, their major ceramides were dLCB-NFAs/HFAs, but tLCB-NFAs/HFAs are very minor, suggesting that once GlcCers with dLCB are synthesized in the kidneys they are converted to LacCers through the actions of the GlcCer transfer protein FAPP2 [51, 52] and LacCer synthase [53]; this trend is more obvious for dLCB-NFAs than for dLCB-HFAs. Most GlcCers with tLCBs and LacCers with dLCB-HFAs stayed as GlcCers and LacCers themselves. As sugar elongation proceeds from LacCers to the globo-series GSLs, the ceramides of dLCB-NFAs become dominant. Gb3Cers were composed of 22 species including five ceramides with NOD-LCBs (d16:1, d17:1 and t20:0) and their major ceramides were dLCB-NFAs. Although Gb4Cers and Forssman glycolipids were composed of only nine species of dLCB-NFAs, they had the characteristic major species d18:1-C24:0 and d18:1-C24:1, the latter of which was minor in their precursor GSLs, with reciprocal reduction of species with C16:0 and C18:0. To exclude the possibility that such a preference of ceramide species is artificial because of different levels of ion intensities, we converted Gb3Cers to LacCers by digestion with α-galactosidase, and Forssman glycolipids to Gb3Cers through Gb4Cers by sequential digestions with α-N-acetylgalatosaminidase and β-N-acetylhexosaminidase, and analyzed them by MALDI-TOF MS and HPTLC. As shown in Supplemental Fig. V, the compositions of the digested GSLs are very similar to the original ones. In addition, while the Gb3Cers from equine kidneys showed triple bands (probably the upper, middle and lower bands are composed of Gb3Cer with d18:1-C24:0, Gb3Cer with d18:1-C22:0/C20:0, and Gb3Cer with d18:1-C16:0, respectively), Forrsman glycolipids showed a single band probably due to the predominance of d18:1-C24:1/C24:0 (Supplemental Fig. V). These results clearly indicated the preference of ceramide species, according to proceeding

glycosylation in the GSLs. NOD-LCBs were detected mostly in the free ceramides, and as glycosylation advances, they become less abundant and are not detected in Gb4Cers and Forssman glycolipids. Because we could not know the exact differences in diagnostic ion intensities between the sphingolipids with OD-LCBs and those with NOD-LCBs, lower abundance of the GSLs with NOD-LCBs may be due to differences in these ion intensities. However, this is unlikely because all of the isomeric sphingolipids we found in this experiment are relatively similar in terms of their structures, suggesting similar ion intensities among them. The differences between them are limited to a single $-CH_2-$ or $-(CH_2)_2-$ in the alkyl chain length of either the FA or the LCB. Isomeric sphingolipids exhibiting a difference of $-(CH_2)_n-$, where $n=3$ or larger, were not found in this experiment. Although it is still theoretically possible that ion intensities from such lipids are extremely low, this is supposed to be unlikely. Among the NOD-LCBs, d16:1 and d20:1 are major LCBs. It was reported that gangliosides containing d20:1 were accumulated in the mouse hippocampus during aging [54]. Likewise, the sphingolipids containing NOD-LCBs may exhibit specific functions in the kidneys, even though they are minor. These results likely reflect the fact that different types of cells utilize specific ceramide species according to their individual functions. In addition, these results may also reflect in part the substrate preferences of FAPP2 and/or the glycosyltransferases, although these possibilities have not been reported.

Combining free ceramides and the constituent ceramides in GSLs in the equine kidneys, we detected a total of 80 ceramide species. Interestingly, we could not detect one type of ceramide, namely d0LCB with unsaturated fatty acid such as d18:0-C16:1. Because it is premature to conclude the absence of such ceramide species as d18:0-Cn:1, careful attention to the presence or absence of such species should continuously be paid for better understanding of sphingolipid metabolism.

Our method can be applied to free ceramides and constituent ceramides in neutral GSLs including those with longer oligosaccharides such as Forrsman glycolipid, being governed by the same principles used for the characterization of free ceramide species. We believe that this systematic approach can help address unanswered subjects regarding not only the metabolism but also the functions of sphingolipids including GSLs.

References

1. Hirabayashi, Y., Igarashi, Y., Merrill Jr., A.H.: Sphingolipids synthesis, transport and cellular signaling. In: Hirabayashi, Y., et al. (eds.) Sphingolipid Biology, pp. 3–22. Springer, Tokyo (2006)
2. Hannun, Y.A., Obeid, L.M.: Principles of bioactive lipid signalling: lessons from sphingolipids. Nat. Rev. Mol. Cell Biol. **9**, 139–150 (2008)
3. Regina Todeschini, A., Hakomori, S.I.: Functional role of glycosphingolipids and gangliosides in control of cell adhesion, motility, and growth, through glycosynaptic microdomains. Biochim. Biophys. Acta. **1780**, 421–433 (2008)
4. Yu, R.K., Yanagisawa, M.: Glycosignaling in neural stem cells: involvement of glycoconjugates in signal transduction modulating the neural stem cell fate. J Neurochem. **103**(Suppl 1), 39–46 (2007)
5. Masukawa, Y., Narita, H., Shimizu, E., Kondo, N., Sugai, Y., Oba, T., Homma, R., Ishikawa, J., Takagi, Y., Kitahara, T., Takema, Y., Kita, K.: Characterization of overall ceramide species in human stratum corneum. J. Lipid Res. **49**, 1466–1476 (2008)
6. Kyogashima, M., Tadano-Aritomi, K., Aoyama, T., Yusa, A., Goto, Y., Tamiya-Koizumi, K., Ito, H., Murate, T., Kannagi, R., Hara, A.: Chemical and apoptotic properties of hydroxyceramides containing long-chain bases with unusual alkyl chain lengths. J Biochem. **144**, 95–106 (2008)
7. Panasiewicz, M., Domek, H., Hoser, G., Kawalec, M., Pacuszka, T.: Structure of the ceramide moiety of GM1 ganglioside determines its occurrence in different detergent-resistant membrane domains in HL-60 cells. Biochemistry **42**, 6608–6619 (2003)
8. Panasiewicz, M., Domek, H., Hoser, G., Fedoryszak, N., Kawalec, M., Pacuszka, T.: The ceramide structure of GM1 ganglioside differently affects its recovery in low-density membrane fractions prepared from HL-60 cells with or without triton-X100. Cell Mol Biol Lett. **14**, 175–189 (2009)
9. Buschard, K., Blomqvist, M., Månsson, J.E., Fredman, P., Juhl, K., Gromada, J.: C16:0 sulfatide inhibits insulin secretion in rat beta-cells by reducing the sensitivity of KATP channels to ATP inhibition. Diabetes **55**, 2826–2834 (2006)
10. Iwabuchi, K., Prinetti, A., Sonnino, S., Mauri, L., Kobayashi, T., Ishii, K., Kaga, N., Murayama, K., Kurihara, H., Nakayama, H., Yoshizaki, F., Takamori, K., Ogawa, H., Nagaoka, I.: Involvement of very long fatty acid-containing lactosylceramide in lactosylceramide-mediated superoxide generation and migration in neutrophils. Glycoconj J. **25**, 357–374 (2008)
11. Mahfoud, R., Manis, A., Lingwood, C.A.: Fatty acid-dependent globotriaosyl ceramide receptor function in detergent resistant model membranes. J. Lipid Res. **50**, 1744–1755 (2009)
12. Hsu, F.F., Turk, J.: Characterization of ceramides by low energy collisional-activated dissociation tandem mass spectrometry with negative-ion electrospray ionization. J. Am. Soc. Mass Spectrom. **13**, 558–570 (2002)
13. Gu, M., Kerwin, J.L., Watts, J.D., Aebersold, R.: Ceramide profiling of complex lipid mixtures by electrospray ionization mass spectrometry. Anal. Biochem. **244**, 347–356 (1997)
14. Bielawski, J., Pierce, J.S., Snider, J., Rembiesa, B., Szulc, Z.M., Bielawska, A.: Comprehensive quantitative analysis of bioactive sphingolipids by high-performance liquid chromatography-tandem mass spectrometry. Methods Mol. Biol. **579**, 443–467 (2009)
15. Ikeda, K., Shimizu, T., Taguchi, R.: Targeted analysis of ganglioside and sulfatide molecular species by LC/ESI-MS/MS with theoretically expanded multiple reaction monitoring. J. Lipid Res. **49**, 2678–2689 (2008)
16. Haynes, C.A., Allegood, J.C., Park, H., Sullards, M.C.: Sphingolipidomics: methods for the comprehensive analysis of sphingolipids. J. Chromatogr. B **877**, 2696–2708 (2009)
17. Scherer, M., Leuthaeuser-Jaschinski, K., Ecker, J., Schmitz, G., Liebisch, G.: A rapid and quantitative LC-MS/MS method to profile sphingolipids. J. Lipid Res. **51**, 2001–2011 (2010)

18. Levery, S.B.: Glycosphingolipid structural analysis and glycosphingolipidomics. Methods Enzymol. **405**, 300–369 (2005)
19. Kyogashima, M., Tamiya-Koizumi, K., Ehara, T., Li, G., Hu, R., Hara, A., Aoyama, T., Kannagi, R.: Rapid demonstration of diversity of sulfatide molecular species from biological materials by MALDI-TOF MS. Glycobiology **16**, 719–728 (2006)
20. Nakamura, K., Suzuki, Y., Goto-Inoue, N., Yoshida-Noro, C., Suzuki, A.: Structural characterization of neutral glycosphingolipids by thin-layer chromatography coupled to matrix-assisted laser desorption/ionization quadrupole ion trap time-of-flight MS/MS. Anal. Chem. **78**, 5736–5743 (2006)
21. Ohta, M., Matsuura, F., Henderson, G., Laine, R.A.: Novel free ceramides as components of the soldier defense gland of the Formosan subterranean termite (Coptotermes formosanus). J. Lipid Res. **48**, 656–664 (2007)
22. Parry, S., Ledger, V., Tissot, B., Haslam, S.M., Scott, J., Morris, H.R., Dell, A.: Integrated mass spectrometric strategy for characterizing the glycans from glycosphingolipids and glycoproteins: direct identification of sialyl Le(x) in mice. Glycobiology **17**, 646–654 (2007)
23. Nagahori, N., Abe, M., Nishimura, S.: Structural and functional glycosphingolipidomics by glycoblotting with an aminooxy-functionalized gold nanoparticle. Biochemistry **48**, 583–594 (2009)
24. Hara, A., Taketomi, T.: Long chain base and fatty acid compositions of equine kidney sphingolipids. J. Biochem. **78**, 527–536 (1975)
25. Rumsby, M.G.: A modified column chromatographic method for the recovery of the glycerogalactolipid fraction of nerve tissue. Some observations on the fractionation of nerve tissue glycolipids on silicic acid with chloroform and acetone mixtures. J. Chromatogr. **42**, 237–247 (1969)
26. Tomita, M., Taguchi, R., Ikezawa, H.: Molecular properties and kinetic studies on sphingomyelinase of Bacillus cereus. Biochim. Biophys. Acta. **704**, 90–99 (1982)
27. Saito, T., Hakomori, S.I.: Quantitative isolation of total glycosphingolipids from animal cells. J. Lipid Res. **12**, 257–259 (1971)
28. Hara, A., Kitazawa, N., Taketomi, T.: Abnormalities of glycosphingolipids in mucopolysaccharidosis type III B. J. Lipid Res. **25**, 175–184 (1984)
29. Courtois, J.E., Petek, F.: α-Galatosidase from coffee beans. Methods Enzymol. **8**, 565–571 (1966)
30. Kadowaki, S., Ueda, T., Yamamoto, K., Kumagai, H., Tochikura, T.: Isolation and characterization of a blood group A substance-degrading α-*N*-acetylgalactosaminidase from an *Acremonium* sp. Agric. Biol. Chem. **53**, 111–120 (1989)
31. Li, S.C., Li, Y.T.: Studies on the glycosidases of jack bean meal. 3. Crystallization and properties of beta-N-acetylhexosaminidase. J. Biol. Chem. **245**, 5153–5160 (1970)
32. Pouria, S., Corran, P.H., Smith, A.C., Smith, H.W., Hendry, B.M., Challacombe, S.J., Tarelli, E.: Glycoform composition proWling of O-glycopeptides derived from human serum IgA1 by matrix-assisted laser desorption ionization-time of Xight-mass spectrometry. Anal. Biochem. **330**, 257–263 (2004)
33. Matsuda, J., Kido, M., Tadano-Aritomi, K., Ishizuka, I., Tominaga, K., Toida, K., Takeda, E., Suzuki, K., Kuroda, Y.: Mutation in saposin D domain of sphingolipid activator protein gene causes urinary system defects and cerebellar Purkinje cell degeneration with accumulation of hydroxy fatty acid-containing ceramide in mouse. Hum. Mol. Genet. **13**, 2709–2723 (2004)
34. Costello, C.E., Vath, J.E.: Tandem mass spectrometry of glycolipids. Methods Enzymol. **193**, 738–768 (1990)
35. Domonand, B., Costello, C.E.: A systematic nomenclature for carbohydrate fragmentations in FAB-MS/MS spectra of glycoconjugates. Glycoconj. J. **5**, 397–409 (1988)
36. Signorelli, P., Munoz-Olaya, J.M., Gagliostro, V., Casas, J., Ghidoni, R., Fabriàs, G.: Dihydroceramide intracellular increase in response to resveratrol treatment mediates autophagy in gastric cancer cells. Cancer Lett. **282**, 238–243 (2009)
37. Adams, J., Gross, M.L.: Charge-remote fragmentations of closed-shell Ions. A thermolytic analogy. J. Am. Chem. Soc. **111**, 435–440 (1989)
38. Harvey, D.J.: A new charge-associated mechanism to account for the production of fragment ions in the high-energy CID spectra of fatty acids. J. Am. Soc. Mass Spectrom. **16**, 280–290 (2005)
39. Qinghong, A., Adams, J.: Structure-specific collision-induced fragmentations of ceramides cationized with alkali-metal ions. Anal. Chem. **65**, 7–13 (1993)
40. Adams, J., Qinghong, A.: Structure determination of sphingolipids by mass spectrometry. Mass Spectrum. Rev. **12**, 51–85 (1993)
41. Ohashi, Y., Iwamori, M., Ogawa, T., Nagai, Y.: Analysis of long-chain bases in sphingolipids by positive ion fast atom bombardment or matrix-assisted secondary ion mass spectrometry. Biochemistry **26**, 3990–3995 (1987)
42. Kurogochi, M., Nishimura, S.-I.: Structural characterization of N-glycopeptides by matrix-dependent selective fragmentation of MALDI-TOF/TOF tandem mass spectrometry. Anal. Chem. **76**, 6097–6101 (2004)
43. Stahl, B., Steup, M., Karas, M., Hillenkamp, F.: Analysis of neutral oligosaccharides by matrix-assisted laser desorption/ionization mass spectrometry. Anal. Chem. **63**, 1463–1466 (1991)
44. Karlsson, K.A., Steen, G.O.: Studies on sphingosines. 13. The existence of phytosphingosine in bovine kidney sphingomyelins. Biochim. Biophys. Acta. **152**, 798–800 (1968)
45. Breimer, M.E., Karlsson, K.A., Samuelsson, B.E.: Presence of phytosphingosine combined with 2-hydroxy fatty acids in sphingomyelins of bovine kidney and intestinal mucosa. Lipids. **10**, 17–19 (1975)
46. Karlsson, K.A., Nilsson, K., Samuelsson, B.E., Steen, G.O.: The presence of hydroxy fatty acids in sphingomyelins of bovine rennet stomach. Biochim. Biophys. Acta. **176**, 660–663 (1969)
47. Kitano, Y., Iwamori, Y., Kiguchi, K., DiGiovanni, J., Takahashi, T., Kasama, K., Niwa, T., Harii, K., Iwamori, M.: Selective reduction in alpha-hydroxypalmitic acid-containing sphingomyelin and concurrent increase in hydroxylated ceramides in murine skin tumors induced by an initiation-promotion regimen. Jpn. J. Cancer Res. **87**, 437–441 (1996)
48. Robinson, B.S., Johnson, D.W., Poulos, A.: Novel molecular species of sphingomyelin containing 2-hydroxylated polyenoic very-long-chain fatty acids in mammalian testes and spermatozoa. J. Biol. Chem. **267**, 1746–1751 (1992)
49. Morell, P., Radin, N.S.: Synthesis of cerebroside by brain from uridine diphosphate galactose and ceramide containing hydroxy fatty acid. Biochemistry **8**, 506–512 (1969)
50. Schaeren-Wiemers, N., van der Bijl, P., Schwab, M.E.: The UDP-galactose:ceramide galactosyltransferase: expression pattern in oligodendrocytes and Schwann cells during myelination and substrate preference for hydroxyceramide. J. Neurochem. **65**, 2267–2278 (1995)
51. D'Angelo, G., Polishchuk, E., Di Tullio, G., Santoro, M., Di Campli, A., Godi, A., West, G., Bielawski, J., Chuang, C.C., van der Spoel, A.C., Platt, F.M., Hannun, Y.A., Polishchuk, R.,

Mattjus, P., De Matteis, M.A.: Glycosphingolipid synthesis requires FAPP2 transfer of glucosylceramide. Nature **449**, 62–67 (2007)

52. Halter, D., Neumann, S., van Dijk, S.M., Wolthoorn, J., de Mazière, A.M., Vieira, O.V., Mattjus, P., Klumperman, J., van Meer, G., Sprong, H.: Pre- and post-Golgi translocation of glucosylceramide in glycosphingolipid synthesis. J. Cell Biol. **179**, 101–115 (2007)
53. Chatterjee, S.: Assay of lactosylceramide synthase and comments on its potential role in signal transduction. Methods Enzymol. **311**, 73–81 (2000)
54. Sugiura, Y., Shimma, S., Konishi, Y., Yamada, M.K., Setou, M.: Imaging mass spectrometry technology and application on ganglioside study; visualization of age-dependent accumulation of C20-ganglioside molecular species in the mouse hippocampus. PLoS One. **3**, e3232 (2008)